SHARING

SELF-ORGANIZED HETEROGENEOUS ADVANCED RADIO NETWORKS GENERATION

Deliverable D3.4

Flexible Interference Management Concept: Innovative Concepts and Performance Evaluation

Date of delivery	31/01/2015
Contractual date of delivery	31/01/2015
Project number	C2012/1-8
Editor(s)	Paul de Kerret (EUR)
Author(s)	Xinping Yi (EUR), Paul de Kerret (EUR), David Gesbert (EUR), Gregory Gougeon (SIR), Mathieu Brau (SIR), Yves Lostanlen (SIR), Fatima Zohra Kaddour (CEA), Benoît Denis (CEA), Dimitri Ktenas (CEA), Sylvie Mayrargue (CEA), Raphael Visoz (Orange), Yasser Fadlallah (Orange), Antoine Berthet (SUPELEC)
Dissemination level	PU
Workpackage	3
Total number of pages	46

Abstract:

This deliverable evaluates innovative interference handling methods and provides first simulation results to show their practical interest. One of the main focus consists in the development of interference management methods being adapted to the practical constraints encountered in realistic networks and exploiting in the most efficient manner the resources available. Hence, transmissions schemes achieving good performances at the cost of only limited Channel State Information (CSI) at the transmitters are proposed. A channel modelling approach is also proposed to serve as a building block to provide the interference management schemes with more accurate knowledge of the channel state. Finally, a novel abstraction framework is presented to optimize the limited CSI feedback in presence of turbo Linear CodeWord Interference Cancellation (turbo L-CWIC) receiver architecture.

Keywords: interference management, interference avoidance, interference alignment, interference cancellation

TABLE OF CONTENTS

1 EXECUTIVE SUMMARY 6

2 INTRODUCTION 8

3 INTERFERENCE MANAGEMENT WITH IMPERFECT CHANNEL FEEDBACK 10

3.1 INTERFERENCE ALIGNMENT WITH INCOMPLETE CSIT 10
3.1.1 Introduction 10
3.1.2 System Model 10
3.1.3 Interference Alignment with Incomplete CSIT for Tightly-Feasible Channels 12
3.1.4 Interference Alignment with Incomplete CSIT for Super-Feasible Channels 13
3.1.5 Simulation Results 14
3.1.6 Conclusion 15
3.2 INTERFERENCE MANAGEMENT WITH TOPOLOGICAL CSIT 17
3.2.1 Introduction 17
3.2.2 Problem Description 17
3.2.3 A Graph Theoretic Perspective 18
3.2.4 An Interference Alignment Perspective 20
3.2.5 Conclusion 22

4 INTERFERENCE MANAGEMENT WITH REALISTIC CHANNEL MODELLING 23

4.1 REALISTIC CHANNEL MODELLING AND NETWORK SIMULATION 23
4.2 JOINT LOCATION AND INTERFERENCE PREDICTION FOR ICIC 25
4.2.1 Statistical interference estimation state of the art – Stochastic approach 27
4.2.2 Considered assumptions and scenario 28
4.2.3 Location-dependent inter-cell interference estimation 30
4.2.4 Location-dependent ICI mapping performance evaluation 32
4.2.5 Conclusion and future work 34

5 CALIBRATION FRAMEWORK FOR PHYSICAL LAYER ABSTRACTION OF (TURBO) CODEWORD IC RECEIVERS 36

5.1 INTRODUCTION 36
5.2 SYSTEM MODEL 36
5.3 LAPPR-BASED TURBO L-CWIC 37
5.3.1 Turbo L-CWIC architecture 37
5.3.2 PHY abstraction 37
5.4 PHY ABSTRACTION CALIBRATION 38
5.4.1 Calibration methods 38
5.5 SIMULATION RESULTS 40

6 CONCLUSIONS 43

LIST OF FIGURES

Figure 1: Average rate per user in terms of the normalized TX power for the tightly-feasible IC 14
Figure 2: CSIT allocation size for K = 3 users. 15
Figure 3: A topology of the 6-cell network. 20
Figure 4: Illustration for a regular cellular network. 22
Figure 5: Macro-cell layer deployment in a real dense urban environment. 23
Figure 6: Cell selection (left) and received power from selected cell (right). 24
Figure 7: Interference map. 25
Figure 8: Space/time interference prediction. 26
Figure 9: Cumulative distribution function of inter-cell interference level in regular and random network. 27
Figure 10: Two-tier heterogeneous network realization 29
Figure 11: Observation zone containing the more interfering BSs. 30
Figure 12: Co-tier Interference map in Macro cell scenario. 33
Figure 13: Co-tier analytical and simulated maps. 34
Figure 14: Relative co-tier interference error 34
Figure 15: STBICM transmission scheme within a FLA framework. 36
Figure 16: PHY abstraction for turbo L-CWIC at iteration *i*. 38
Figure 17: Batch of curves stocked in the Trace files in order to perform the calibration for MCS 6 and MCS12. 41
Figure 18: The convergence of the 3D MSE calibration solution for MCS 6 and MCS 12. 42
Figure 19: Comparison of the predicted and simulated PER for MCS 6 and MCS 12. 42

LIST OF TABLES

Table 1: Link scheduling 19
Table 2: 8-block fading channel - 1D/3D calibration factors 40
Table 3: 1-block fading channel - MSE 40
Table 4: 1-block fading MSE w.r.t. the calibration coefficients optimized for 8-block fading channel 42

ACRONYM	DEFINITION
3GPP	Third Generation Partnership Project
AWGN	Additive White Gaussian Noise
BER	Bit Error Rate
BPP	Binomial Point Process
BS	Base Station
CDF	Cumulative Distribution Function
CoMP	Coordinated Multi-Point
CSI	Channel State Information
CSIT	Channel State Information at Transmitter
DL	Downlink
DoF	Degree of Freedom
eNB	evolved Node B
FDD	Frequency Division Duplex
FLA	Fast Link Adaptation
HetNET	HETerogeneous NETwork
IA	Interference Alignment
IC	Interference Channel
ICI	Inter-Cell Interference
ICIC	Inter-Cell Interference Coordination
IER	Interference Estimation Reliability
ISD	Inter-Site Distance
JP	Joint Processing
LMMSE	Linear Minimum Mean Square Error
LTE-A	Long Term Evolution - Advanced
MAC	Media Access Control
MCSs	Modulation and Coding Schemes
MIMO	Multiple Input Multiple Output
ML	Maximum Likelihood
MSE	Mean Square Error
NLOS	Non Line-Of-Sight
OFDMA	Orthogonal Frequency Division Multiplexing Access
PDF	Probability Distribution Function
PER	Packet Error Rate
PHY	PHYsical Layer
PPP	Poisson Point Process

QoS	Quality of Service
RE	Resource Element
RX	Receiver
RRM	Radio Resource Management
SINR	Signal to Interference plus Noise Ratio
SNR	Signal to Noise Ratio
TIM	Topological Interference Management
TTI	Transmission Time Interval
TX	Transmitter
UE	User Equipment
ZF	Zero Forcing

1 EXECUTIVE SUMMARY

Interference represents a bottleneck in the spectrum efficiency of modern dense wireless networks. This document presents several innovative concepts and algorithmic solutions which aim at helping the receiver getting rid of unwanted interference, via an intelligent design at the transmitter side.

Section 3 discusses the need for efficient interference management schemes in order to achieve the desired Quality-Of-Service (QoS) of future wireless networks. It is shown that an ideal interference management can only be done if the network has sufficient resources in terms of feedback, backhaul links, signal processing capabilities, etc. This leads to the fact that novel innovative methods are needed so as to adapt to the practically encountered scenarios in which insufficient resources are available. Achieving most of the gains of interference management in practical settings with only limited resources is very challenging and is the main focus of this deliverable. Section 3 challenges the usual assumption of full channel state information at the transmitters. Hence, the benefits of some interference management techniques such as interference avoidance and interference alignment are investigated under partial availability of channel knowledge at transmitters. In particular, it is shown that interference alignment does not always require full knowledge of the multi-user channel. Another interesting scenario occurs when transmitters only have access to the topological information. It is then shown how this information can significantly improve the performance in comparison to the situation without any channel information. More details can be found on the journal publications which have resulted from these work [KG14, YG14].

Section 4 presents novel methods to obtain accurate models predicting the level of interference experienced by the users. First, a ray tracing approach is developed based on results from the realistic simulation framework introduced in [D3.1]. It is then shown how realistic interference maps can be obtained in a dense urban environment from a ray-based propagation model. Further processing of these interference maps allows to assess network performance and to generate inputs that can be used for radio resource management algorithms. An alternative probabilistic approach is then described. A new analytical model based on stochastic geometry, which predicts the Inter-cell Interference (ICI) level suffered by User Equipment's (UEs) in Downlink (DL) in Heterogeneous Networks (HetNets) according to their location. The HetNet is modelled using stochastic geometry. More specifically, the proposed model relies on the Poisson Point Process (PPP) formalism (and its large arsenal of tools) to derive closed forms for location-dependent ICI under realistic propagation channel assumptions, including both fast fading and shadowing. Same and separate frequency band allocations are investigated for macro and small cells, leading to co-channel and co-tier interference respectively. Analytical models are derived regarding interference median value. These predictions are used to build 2D interference maps (i.e. with estimated ICI level at each pixel of the area of interest), which could be subsequently beneficial to location-based Radio Resource Management (RRM) or ICI coordination/cancellation algorithms in real systems. We provide illustrations in Long Term Evolution-Advanced (LTE-A) standard-compliant scenarios, while discussing the ”spatial reliability” of this model.

Section 5 presents and discusses a novel calibration framework for physical layer abstraction of (turbo) Codeword IC receivers. Modern wireless communication systems rely on limited feedback for Fast Link Adaptation (FLA). FLA in presence of advanced receivers needs new Physical layer abstractions (PHY abstractions) that are able to capture their performance in order to derive the limited feedback metrics (e.g., channel quality indicators). Recently, a PHY abstraction was proposed for the class of iterative linear minimum mean square error based soft interference cancellation and decoding also referred to as turbo Linear Codeword Interference Cancellation (turbo L-CWIC) receivers in Third Generation Partnership Project (3GPP) [3GPP12]. This PHY abstraction needs to be calibrated and a first one-dimensional (1D) calibration method was proposed. In this study, we revisit the calibration method by proposing a more rigorous framework to minimize the predicted throughput error that dramatically

bias the FLA mechanisms. We also suggest a novel multi-dimensional calibration approach. Monte Carlo simulations show that it outperforms the 1D calibration at the expense of the knowledge of the number of independent fading blocks experienced by a codeword.

Finally, the main conclusions of this deliverable are presented and considered in the broader perspective of the project. The undergoing works are outlined and the next steps are presented.

2 INTRODUCTION

In order to deal with the fast increasing demand for new wireless (multimedia) services, new wireless systems are designed based on greater densification of infrastructure equipments (small cells), and a very aggressive spatial frequency reuse. Spatial reuse of resources in turn results in severe interference conditions especially for cell-edge terminals [GHH10].

The role played by interference control methods in this context is critical so as to provide the users with the required quality of service. Interference control methods can be categorized according to where intelligent algorithms are mostly located. In interference avoidance methods, intelligence is located mainly at the transmitter side, where the transmitter applies a suitable precoding–based processing before transmitting the data. In the case that multiple (interfering) transmitters jointly optimize their precoding functions, one talks about transmitter cooperation for interference control. At the receiver side, intelligent interference-aware processing can be implemented through the use of interference rejection and/or interference decoding algorithms. Such methods exploit the learned characteristics of the interference signal (for instance the spatial signature, or the codebooks exploited for modulation and coding) to suppress it.

The gain created by multiple antenna combining in mitigating interference by means of ZF (or related criteria) beamforming is well established. The use of multiple antennas allows for extra degrees of liberty for transmitting data while creating nulls in channel directions that correspond to unintended receivers. In the case of transmitter cooperation, devices can jointly design beamforming solutions that, although unable to null out interference at all interfered locations, can align the channel directions followed by distinct interfering sources, making it easier to reject them by a receiving device equipped with just a small number of antennas.

The practical application of above transmitter- or receiver-based interference control mechanisms hinges on the availability of accurate knowledge of CSI. In reality however, most cellular networks are deployed in the Frequency Division Duplex (FDD) mode which requires a dedicated feedback link so as to convey CSI back to the transmitter.

A crucial question then becomes how much interference control capability remains when having to deal with finite CSI accuracy brought by limited feedback. There are several models which have been considered in the literature for limited feedback in the single transmitter case; such as noisy analog, quantized, and delayed feedback. In the case of interference avoidance through transmitter cooperation, an additional model for limited CSI at the transmitter side is referred to as *incomplete* CSI, which indicates that only a part of the global multi-user channel matrix is known at one particular transmitter.

- **Coordinated Multi-Point (CoMP) with Incomplete CSI**

The notion of incomplete CSI is particularly useful in the context of deployment scenarios where it is possible to feedback accurate CSI from terminals to transmitting base station but it is not possible to fully exchange this information across the Base Stations (BS). This may be the case for a latency-prone or rate limited backhaul. Coordinated Multi-Point (CoMP) schemes that can operate with limited CSI are able to mitigate the interference exploiting the channel feedback from only a subset of the users. Such schemes are hereby studied in the context of interference alignment.

- **Interference Control with Topological and Location Dependent Interference**

For scenarios where a high level of mobility is expected from the users, it may not be even practical to rely on instantaneous channel feedback for interference avoidance. A conservative approach then consists in exploiting long term channel gain information. Such information indicates "who interferes with who, strongly or weakly, on average" and is already enough to design interference avoidance schemes as indicated in one of the contributions under this document. More generally it is desirable to gain a better understanding on the macroscopic properties of interference, for instance how the interference power is distributed across the cell as a function of the user location. Such information can among others be

exploited in view of interference power prediction, so as to facilitate resource allocation and/or anticipate handoff functions.

- **Physical LayerPerformance Modelling and Abstractionin the Presence of Interference**

One of the objectives of this document is also related to the design of advanced receiver for handling interference. Advanced receivers are particularly useful when transmitter-based avoidance is imperfect or not possible (for instance in the uplink with single antenna user terminals). For a careful integration of the PHY performance into the link adaptation algorithms, it is important that the interference control capability of the receiver be accounted for in the link adaptation tables. This requires a step of modelling (abstraction) of the PHY performance (e.g., Bit Error Rate (BER)) for various interference and Signal to Noise Ratio (SNR) scenarios. This modelling constitutes the final objective of this document.

3 INTERFERENCE MANAGEMENT WITH IMPERFECT CHANNEL FEEDBACK

3.1 Interference Alignment with Incomplete CSIT

3.1.1 Introduction

Although multi-transmitter coordinated transmission such as Interference Alignment (IA) constitutes a promising tool to combat interference, coordination benefits go at the expense of acquiring accurate enough CSI at the Transmitters (TXs) and sharing it across all TXs whether explicitly or implicitly. In the case of multi-antenna based IA without channel extension, some form of CSI at the TXs (CSIT) is required to compute the precoder at each one of the TXs and can result in a significant overhead in practice. The IA literature for static Multiple Input Multiple Output (MIMO) channels is rich in methods improving the efficiency of the precoding schemes at finite SNR and reducing the complexity of the algorithms. Yet, the obtaining of the CSIT at the TXs represents a major obstacle to its practical use and the study of how CSIT requirements can somehow be alleviated has become an active research topic in its own right.

Yet, in all the existing works on IA feasibility, it is assumed that every TX knows perfectly the full multi-user channel, which we define as the channel from all the TXs to all the Receivers (RXs). This assumption is critical as the maximal Degrees-of-Freedom (DoF) is known to be significantly lower in the absence of CSIT. However, a simple examination of IA achievability in particular cases of Interference Channels (IC) reveals that how much CSIT is required at any one TX actually depends on the antenna configuration. Obvious examples include TXs with single antenna which has no alignment capability, hence requires no CSIT, or an IC with many-antenna RXs which eliminate the need for any alignment, hence CSIT. In the general case with heterogeneous antenna distributions, an interesting question is whether an alignment scheme can get away with less than full CSIT. To this end, one needs to revisit the IA feasibility question under the prism of CSIT. We focus in this task on a completely different problem which is the incomplete CSIT sharing, which means that each TX receives its own CSIT. In particular, we will exploit the fact that some channel coefficients are only known at a subset of TXs. We will show that in this case, perfect alignment is still possible despite the lack of full CSIT. More remarkably, we show that as the number of antennas on the devices (Base Station (BS) and User Equipment (UE)) is increasing, the need for CSIT goes down instead of up as was conventionally thought.

In what follows, we formulate this problem and present the major results. The detailed proof and more results can be found in our journal paper [KG14].

3.1.2 System Model

We study the transmission in a K-user MIMO IC where all the RXs and the TXs are linked by a wireless channel. We consider a conventional channel model with the particularity of our model lying in the structure of the CSIT. We consider that each TX has its own CSIT in the form of a sub-matrix of the multi-user channel matrix. This specific information structure is referred to as incomplete CSIT, which will be detailed later. TX-j is equipped with M_j antennas, RX i has $N_i$antennas, and TX-j transmits a single stream to RXj. This IC is then denoted as $\prod_{k=1}^{K}(N_k, M_k)$. We consider exclusively single-stream transmissions and the extension to multiple streams will be discussed later in this work. When all the TXs and all the RXs have the same (resp. different) number of antennas, i.e., $[(N, M)]^K$, we say that the antenna configuration ishomogeneous (resp. heterogeneous).

The channel from TX j to RXi is represented by the channel matrix $\mathbf{H_{i,j}} \in \mathbb{C}^{N_i \times M_j}$with its elements i.i.d. according to a continuous probability distribution to ensure that all the channel matrices are almost surely full rank. The global multi-user channel matrix is denoted by $\mathbf{H} \in \mathbb{C}^{N_{tot} \times M_{tot}}$ where $N_{tot} \triangleq \sum_{k=1}^{K} N_k$ and $M_{tot} \triangleq \sum_{k=1}^{K} M_k$:

$$\mathbf{H} \triangleq \begin{bmatrix} \mathbf{H_{1,1}} & \cdots & \mathbf{H_{1,K}} \\ \vdots & \ddots & \vdots \\ \mathbf{H_{K,1}} & \cdots & \mathbf{H_{K,K}} \end{bmatrix} \tag{3.1}$$

TXi uses the unit-norm TX beamformer $\mathbf{t}_i \in \mathbb{C}^{M_i \times 1}$ multiplied by$\sqrt{P}$, where P is the transmit power per-TX, to transmit the data symbol s_i (i.i.d.$\mathcal{N}_{\mathbb{C}}(0,1)$) to RX$i$. The received signal $\mathbf{y}_i \in \mathbb{C}^{N_i \times 1}$ at the ith RX reads then as

$$\mathbf{y_i} = \boldsymbol{P}\mathbf{H_{i,i}}\mathbf{t_i} + \boldsymbol{P}\sum_{\mathbf{j=1,j\neq i}}^{\mathbf{K}}\mathbf{H_{i,j}}\mathbf{t_j} + \boldsymbol{\eta}_\mathbf{i} \tag{3.2}$$

where $\eta_i \in \mathbb{C}^{N_i \times 1}$ is the normalized noise at RX-i and is i.i.d. $\mathcal{N}_{\mathbb{C}}(0,1)$. The received signal $\boldsymbol{y}_i$ is then processed by a RX filter $\mathbf{g_i^H} \in \mathbb{C}^{1 \times N_i}$ to obtain an estimate of the data symbolss_i.

Our analysis deals with the achievability of IA, which means that the desired signal should be decoded free of interference at each RX. Equivalently, the RX beamformer $\mathbf{g_i^H}$ should be able to ZF all the received interference which means fulfilling for all the interferers$j \neq i$

$$\mathbf{g_i^H H_{i,j} t_j} = \mathbf{0}. \tag{3.3}$$

Thus, IA is feasible if the above constraint can be achieved at all the RXs for all the interfering streams. Note that this is equivalent to having the interference subspace at RXi span at most $N_i - 1$ dimensions.

- **Incomplete CSIT Model**

The feasibility results from the literature have always made use of an implicit full CSIT assumption. Surprisingly, the problem of revisiting the IA feasibility conditions under the light of a partial CSIT sharing framework has not been addressed before. To fill this gap, it is necessary to introduce a new model to take into account the partial CSIT sharing capability of the TXs.

Hence, we consider that a TX has either perfect knowledge of a channel coefficient or no information at all on that element. We represent the CSIT structure at TX-j by the *CSIT matrix* $\mathbf{A}^{(j)} \in \{0,1\}^{N_{tot} \times M_{tot}}$ such that $\{\mathbf{A}^{(j)}\}_{i,k} = 1$ if $\{\mathbf{H}\}_{i,k}$ is known at TXj, and 0 otherwise. Denoting by $\mathbf{H}^{(j)}$ the available CSI at TX j, we obtain

$$\mathbf{H}^{(j)} = \mathbf{A}^{(j)} \odot \mathbf{H} \tag{3.4}$$

We define the CSIT allocation $\boldsymbol{\mathcal{A}}$ as the set of CSI representations available at all TXs:

$$\mathcal{A} \triangleq \{\mathbf{A}^{(j)} | \mathbf{A}^{(j)} \in \{0,1\}^{\mathrm{N_{tot} \times M_{tot}}}, \mathrm{j} \in \mathcal{K}\} \tag{3.5}$$

and we define the space $\mathbb{A}$ containing all the possible CSIT allocations. We can then define the *size* of an incomplete CSIT allocation as follows.

Definition *(Size of a CSIT Allocation)*: The size of a CSIT allocation $\boldsymbol{\mathcal{A}}$, denoted by $s(\boldsymbol{\mathcal{A}})$, is equal to the overall number of complex channel coefficients fed back to the TXs. Thus,

$$\mathrm{s}(\mathcal{A}) \triangleq \sum_{\mathrm{j=1}}^{\mathrm{K}} \left\| \mathbf{A}^{(\mathrm{j})} \right\|_{\mathrm{F}}^{2}. \tag{3.6}$$

To check whether the IA feasibility is preserved with a given CSIT allocation, we introduce the function f_{feas} which takes as argument a CSIT allocation $\mathbf{A}^{(j)}$ and an antenna configuration $\prod_{k=1}^{K}(N_k, M_k)$ and returns 1 if IA is feasible with these parameters and 0 otherwise. Note that this means that there exists one algorithm achieving IA with this CSIT allocation but it does not precise the algorithm. We also define the set $\mathbb{A}_{\mathrm{feas}}$ containing all the CSIT allocations for which IA is feasible. Hence,

$$\mathbb{A}_{\mathrm{feas}} \triangleq \left\{\mathcal{A} \middle| \mathrm{f_{feas}}\left(\mathcal{A}, \prod_{\mathrm{k=1}}^{\mathrm{K}}(\mathrm{N_k}, \mathrm{M_k})\right)\right\}. \tag{3.7}$$

Note that only the interfering channel matrices $\mathbf{H}_{\mathrm{i,j}}$ with$j \neq i$are required to fulfill the IA constraints, and not the direct channel matrices $\mathbf{H}_{\mathrm{j,j}}$. Thus, from a Degree of Freedom (DoF) point of view, we can always skip the direct channel matrices $\mathbf{H_{j,j}}$ in the feedback, which leads to the following definition.

Definition *(Complete CSIT Allocation)*: A *complete* CSIT allocation, denoted by $\mathcal{A}_{\mathrm{comp}}$, is defined by the knowledge of all the interfering channel matrices $\mathbf{H_{i,j}}$ with $j \neq i$ at all TXs. Thus, the size of a complete CSIT allocation is

$$\boldsymbol{s}\left(\mathcal{A}_{\mathrm{comp}}\right) \triangleq K\left(\mathrm{N_{tot}M_{tot}} - \sum_{\mathrm{i=1}}^{\mathrm{K}} \mathrm{N_i M_i}\right). \tag{3.8}$$

A CSIT allocation with a size smaller than $s(\mathcal{A}_{\text{comp}})$ is said to be *strictly incomplete*.

At this stage, a natural question is to ask what is the most incomplete CSIT allocation which preserves the feasibility of IA, i.e., to find

$$\mathcal{A}_{\min} = \underset{\mathcal{A}\in\mathbb{A}_{\text{feas}}}{\operatorname{argmin}}\, \mathrm{s}(\mathcal{A}). \tag{3.9}$$

Note that we limit here our study to the IA feasible settings, i.e., such that $\mathcal{A}_{\text{comp}} \in \mathbb{A}_{\text{feas}}$.

- **Tightly-feasible and super-feasible settings**

Whether the total number of variables is strictly larger than the number of equations will be shown to impact significantly the CSIT needed. Hence, we introduce the following definitions.

Definition *(Tightly-feasible IC)*: An IC setting is called *tightly-feasible* if this IC is feasible and removing a single antenna at any TX or RX renders IA unfeasible. Equivalently, an IC is tightly-feasible if and only if it is

$$\sum_{\mathrm{i}=1}^{\mathrm{K}} \mathrm{N_i} + \mathrm{M_i} = \mathrm{K}(\mathrm{K}+1). \tag{3.10}$$

Definition *(Super-feasible IC)*: A feasible setting which does not satisfy the tightly-feasible condition is said to be *super-feasible*. Equivalently, a super-feasible setting is a feasible setting such that

$$\sum_{\mathrm{i}=1}^{\mathrm{K}} \mathrm{N_i} + \mathrm{M_i} > K(\mathrm{K}+1). \tag{3.11}$$

3.1.3 Interference Alignment with Incomplete CSIT for Tightly-Feasible Channels

Theorem *(Incomplete CSIT Allocation for Tightly-feasible ICs)*: In a tightly-feasible $\prod_{k=1}^{K}(N_k, M_k)$IC, if a tightly-feasible sub-IC formed by the set of TXs S_{TX} and the set of RXs S_{RX} exists, i.e.,

$$\mathcal{N}_{\text{var}}(\mathrm{S_{RX}}, \mathrm{S_{TX}}) = \mathcal{N}_{\text{eq}}(\mathrm{S_{RX}}, \mathrm{S_{TX}}). \tag{3.12}$$

then the incomplete CSIT allocation $\boldsymbol{\mathcal{A}} \triangleq \{\mathbf{A}^{(j)} | j \in \mathcal{K}\}$ preserves IA feasibility, i.e., $\mathcal{A}_{\text{feas}} \in \mathbb{A}_{\text{feas}}$ if

$$\mathbf{A}^{(\mathrm{j})} = \mathbf{A}_{\mathbf{S_{RX}},\mathbf{S_{TX}}}, \forall \mathrm{j} \in \mathrm{S_{TX}} \tag{3.13}$$

$$\mathbf{A}^{(\mathrm{j})} = \mathbf{A}_{\boldsymbol{\mathcal{K}},\boldsymbol{\mathcal{K}}}, \forall \mathrm{j} \notin \mathrm{S_{TX}} \tag{3.14}$$

This theorem implies that if a tightly-feasible sub-IC strictly included in the considered IC exists, then a strictly incomplete CSIT allocation preserving IA feasibility also exists.

Example: Let us consider as toy-example the $[(2,2),(2,2),(2,2),(4,4)]$ IC. We can easily observe that the first 3 TX/RX pairs form the well-known tightly-feasible $[(2,2)^3]$ IC. Hence, if the 3 first TXs align interference inside this sub-IC, RX4 has then enough antennas to remove all its received interference. In addition, TX4 can use its 4 antennas to eliminate the interference that it emits to the signal subspaces at the first 3 RXs.

In fact, it can be easily seen that the obtained incomplete CSIT allocation exploits the heterogeneity of the antenna configuration. Indeed, there can be a tightly-feasible sub-IC strictly included in a tightly-feasible IC only if the antenna configuration is heterogeneous.

Corollary: In the homogeneous tightly-feasible $[(\mathrm{N},\mathrm{M})^{\mathrm{K}}]$ IC (this implies $\mathrm{M}+\mathrm{N} = \mathrm{K}+1$) with $\mathrm{M} \neq 1$ and $\mathrm{M} \neq \mathrm{K}$, there exists no generalized tightly-feasible sub-IC strictly included in the IC. Hence, the previous sufficient condition leads to no CSIT reduction.

This property only holds for tightly-feasible settings and we will show in the following section that CSIT reductions can be achieved for super-feasible ICs in any antenna configuration. It is then not the antenna heterogeneity, which is exploited, but the additional antennas.

- **An Example**

Let us consider the IC formed by the antenna configuration $[(2,3),(2,4),(3,5),(3,2),(4,2)]$. The CSIT allocation algorithm presented in our paper [KG14] returns

$$\mathcal{A} = \left\{\mathbf{A}^{(1)} = \mathbf{A}_{\{1,2,3\},\{4,5,1\}}, \mathbf{A}^{(2)} = \mathbf{A}_{\{1,2,3,4\},\{1,2,4,5\}}, \mathbf{A}^{(3)} = \mathbf{A}_{\mathcal{K},\mathcal{K}}, \mathbf{A}^{(4)} = \mathbf{A}_{\{1,2\},\{4,5\}}, \mathbf{A}^{(5)} = \mathbf{A}_{\{1,2\},\{4,5\}}\right\} \quad (3.15)$$

We remind the reader that the notation $\mathrm{A}^{(4)} = \mathrm{A}_{\{1,2\},\{4,5\}}$ means that TX4 receives the CSI relative to the sub-IC formed by the TXs in the set {4,5} and the RXs in the set {1,2}.

Hence, TX4 and TX5 have only the CSI sufficient to align their interference at RX1 and RX2, which is in fact the first step of the IA algorithm. Once this is done, TX1 designs its beamformer to align its interference on the interference subspace created by TX4 and TX5 at RX2 and RX3. Note that it has a sufficient CSI to do so. Proceeding further, TX2 aligns its interference on the interference subspace spanned at RX1, RX3, and RX4 by the previous TX beamformers. At this step, all the interference subspaces have been generated and TX3 uses its 5 antennas to align its interference at all the RXs.

The general idea is very simple and reads as follows: The TX beamformers in the smallest tightly-feasible ICs are computed first until all the TX beamformers are computed. Note that the size of the incomplete CSIT allocation obtained in the previous example is equal to 346 while the complete CSIT allocation has a size of 905.

3.1.4 Interference Alignment with Incomplete CSIT for Super-Feasible Channels

The previous section indicates how CSIT savings can be obtained for tightly-feasible scenarios. When additional antennas are available, the intuition goes that further CSIT savings should be possible at no cost in terms of IA feasibility. We now investigate this question.

A distinct feature of super-feasible settings is that there must exist a corresponding tightly-feasible setting that can be obtained by keeping all TXs and RXs and simply ignoring certain antennas among the overall antenna set. Clearly, there are generally multiple ways for arriving at a tightly-feasible setting from a super-feasible one. Depending on the choice of which antennas are ignored in the initial super-feasible setting, the obtained tightly-feasible settings will satisfy particular CSIT requirements. Below, we show how trying to obtain the tightly feasible setting with smaller CSIT allocation in fact leads to the smaller CSIT allocation for the initial super-feasible setting as well.

As a consequence, we consider the following optimization problem:

$$\begin{aligned} \mathcal{A} = \underset{\mathcal{A}}{\operatorname{argmin}} \min_{\prod_{k=1}^{K}(N'_k, M'_k)} & s(\mathcal{A}) \quad (3.16) \\ \text{s.t. } & f_{\text{feas}}\left(\mathcal{A}, \prod_{k=1}^{K}(N'_k, M'_k)\right) = 1 \\ \text{s.t. } & \sum_{i=1}^{K} N'_i + M'_i = K(K+1) \\ \text{s.t. } & 1 \le N'_i \le N_i \\ \text{s.t. } & 1 \le M'_i \le M_i \end{aligned}$$

The problem of finding the minimal CSIT allocation has been reduced to finding the tightly-feasible setting (containing all the users) included in the full super-feasible setting, which requires the smallest CSIT allocation. Since a CSIT allocation algorithm has been derived for tightly-feasible settings, it remains only to determine which RXs or TXs should not fully exploit their antennas to ZF interference dimensions, i.e., where some antennas should be "removed" in terms of IA feasibility.

Practically, the antennas are not removed but some precoding dimensions are used for another purpose than aligning interference inside the IC (e.g., reducing interference to other RXs, increasing signal power, diversity, etc...). As an example, we will now show how it can be used to increase the received signal power. Intuitively, we select the precoding subspace of dimension n with $n < M_i$ which provides the largest received power to the RX. As a consequence, the quality of the direct channel is improved.

The considered optimization problem is combinatorial in the total number of TXs and RXs which makes exhaustive search only practical for small settings. As a consequence, we provide in the following a CSIT allocation policy exploiting heuristically the additional antennas available to reduce the size of the CSIT allocation. The heuristic behind the algorithm comes from the insight gained in the analysis of tightly-feasible settings that the more heterogeneous the antenna configuration is, the smaller the size of the CSIT allocation becomes. Intuitively, our algorithm "removes" the antennas so as to form the "most heterogeneous" antenna configuration where IA remains feasible.

3.1.5 Simulation Results

We start by verifying by simulations that IA is indeed achieved by our new IA algorithm. We consider for the simulations the $[(2,3),(2,4),(3,5),(3,2),(4,2)]$ IC. This example has been chosen to illustrate our approach, but the CSIT reduction is different for each antenna configuration such that it is also relevant to consider the average reduction over all the antenna configurations.

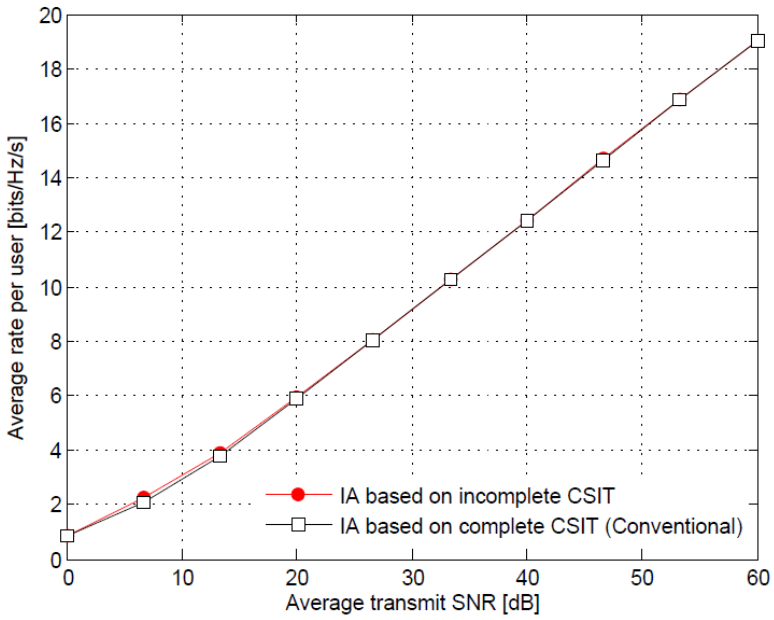

Figure 1: Average rate per user in terms of the normalized TX power for the tightly-feasible IC

We show in Figure 1 the average rate per user achieved in terms of the SNR. We compare then our IA algorithm based on incomplete CSIT to the min-leakage IA algorithm based on complete CSIT. Our algorithm achieves virtually the same performance as the min-leakage algorithm. Hence, the reduction of 60% of the feedback size comes for "free", making it especially interesting in practice.

We will now evaluate the feedback reduction obtained with our CSIT allocation policy in super-feasible settings. Since this gain depends on the antenna configuration, we show Figure 2 the average size of the CSIT allocation for K=3 users when the antennas are allocated at random to the TXs and the RXs according to the uniform distribution. Note that the antenna configurations obtained can make IA unfeasible. When this is the case, we redistribute the antennas until a feasible antenna configuration is obtained.

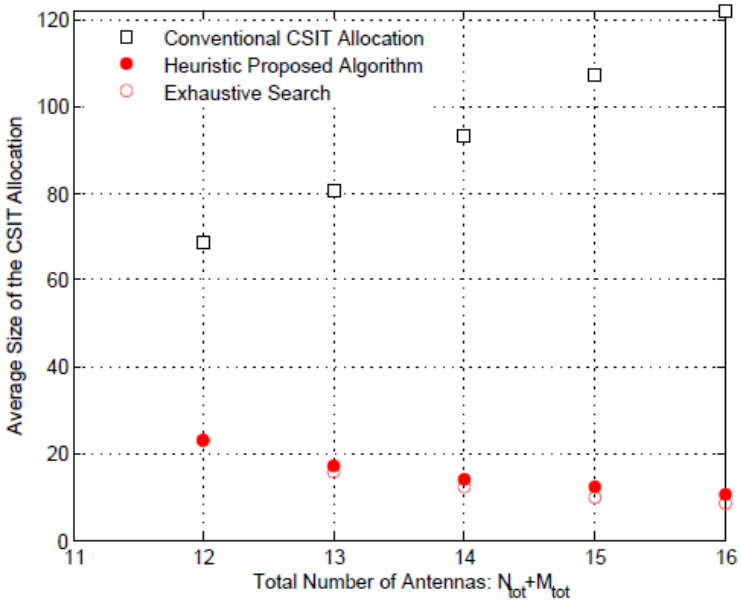

Figure 2: CSIT allocation sizefor K = 3 users.

We average over 1000 antenna configurations and the proposed heuristic CSIT allocation policy is compared with the exhaustive search. The exhaustive search consists in testing all the possibilities for removing the additional antennas. For reference, we also show the average size of the complete (conventional) CSIT allocation. We consider only K=3 users because of the exponential complexity of the exhaustive search.

If the aggregate number of antennas is strictly smaller than $K(K+1) = 12$, it follows that IA cannot be feasible. The result obtained with 12 antennas distributed between all the nodes corresponds then to the tightly-feasible case. It is hence possible to observe how our CSIT allocation algorithm leads to a significant reduction of the required CSIT without requiring any additional antenna. If more than 12 antennas are available, each additional antenna is exploited by the heuristic algorithm to reduce the size of the CSIT allocation. This algorithm brings a reduction of the CSIT size which is only slightly smaller than the reduction brought by exhaustive search, but has a polynomial complexity. Note that allocating the antennas uniformly at random represents a worst case as it tends to generate homogeneous settings as the number of antennas increases.

3.1.6 Conclusion

IA feasibility is studied in the literature under the assumption of full CSIT sharing. In contrast, the relation between IA feasibility and CSIT allocation is investigated in this work. Specifically, it is shown how IA can be achieved in some cases without full CSIT sharing. When extra-antennas are available, the existence of a trade-off between the number of antennas available and the CSIT sharing requirements is shown. Our approach brings a significant reduction of the feedback size while introducing no losses in terms of DoF compared to the conventional IA algorithm with full CSIT sharing.

Furthermore, IA with incomplete CSIT sharing raises additional interesting open problems that go beyond the scope of this section. Firstly, proving the minimality of our reduced CSIT allocation (or finding the minimal CSIT allocation policy) could not be achieved due to the difficulty in deriving a lower bound for the minimal size of a CSIT allocation preserving IA feasibility. Another interesting problem is to extend the study to multiple streams transmissions. Verifying IA feasibility represents already a difficult problem in this case so that the derivation of analytical results is challenging. However, the main idea behind our CSIT allocation algorithm directly extends to the general case with multiple-stream transmissions.

Finally, the analysis has been carried out by considering the DoF which models the performance at asymptotically high SNR. At low to medium SNR, it is expected that CSIT incompleteness will lead to some

rate loss as beamforming capabilities are reduced. Thus, an interesting problem lies in the trade-off between CSIT sharing reduction and finite SNR rate performance.

3.2 Interference Management with Topological CSIT

3.2.1 Introduction

Most known techniques for interference coordination and cooperation (such as interference alignment, coordinated beamforming and Joint Processing (JP)-CoMP) rely on the assumption that the transmitters are endowed with an instantaneous form of channel information whose coherence time is similar to that of the actual fading channels, so that a good fraction or the totality of the DoF achieved in the perfect CSIT can be obtained. Such an assumption is hard to realize in many practical scenarios. A closer examination of these pessimistic results however reveals that many of the considered networks are fully connected, in that any transmitter interferes with any non-intended receiver in the network.

Owing to the nodes' random placement, the fact that power decays fast with distance, the existence of obstacles and local shadowing effects, certain interference links are unavoidably much weaker than others, suggesting the use of a partially-connected graph to model, at least approximately, the network topology. An interesting question then arises as to whether the partial connectivity could be leveraged to allow the use of some relaxed form of CSIT while still achieving a substantial DoF performance. In particular the exploitation of topological information, simply indicating which of the interfering links are weak enough to be approximated by zero interference and which links are too strong to do so, is of great practical interest. This problem was formulated in a partially connected interference channel, where the transmitters know only network topology but without knowing channel realizations, under the name of "topological interference management (TIM) [JAF14]".

The objective of this task is to answer the question whether such topological information can somehow be exploited in the context of an interference network where a message exchange mechanism between transmitters pre-exists. For instance, in future LTE-A cellular networks, a backhaul routing mechanism ensures that base stations selected to cooperate under the CoMP framework receive a copy of the messages to be transmitted. Still, the exchange of timely CSI is challenging due to the rapid obsolescence of instantaneous CSI and the latency of backhaul signalling links. In this case, a broadcast channel over distributed transmitters (a.k.a. network MIMO) ensues, with no instantaneous CSIT.

The problem raised by this task concerns the use of topology information in this setting. In what follows, we formulate this problem and present some interesting results in brief. The detailed proof as well as more results can be found in our journal paper [YG14].

3.2.2 Problem Description

We consider a network with K TXs e.g. cells. In each cell the TX (e.g. base station) is equipped with one antenna and serves one single-antenna RX. The partial connectivity of the network is modelled through the received signal equation for RX-j at time instant t by:

$$\mathbf{Y_j(t)} = \sum_{\mathbf{i}\in\mathcal{T}_\mathbf{j}} \mathbf{h_{j,i}X_i(t)} + \mathbf{Z_j(t)} \qquad (3.17)$$

where $h_{i,j}(t)$ is the channel coefficient between TXi and RXj, the transmitted signal $X_i(t)$ is subject to the individual power constraint, i.e., $E[|X_i(t)|^2] \le P$, with Pbeing average transmit power, and $Z_j(t)$ is the Gaussian noise with zero-mean and variance N0 and is independent of transmitted signals and channel coefficients. We denote by $\mathcal{T}_k$the transmit set containing the indices of transmitters that are connected to RXk, and by $\mathcal{R}_k$ the receive set consisting of the indices of receivers that are connected to TX k. In practice the partial connectivity may be modelled by taking those interference links that are "weak enough" (due to distance and/or shadowing) to zero.

Conforming to the so-called Topological Interference Management (TIM) framework, the actual channel realizations are not available at the transmitters, yet the network topology (i.e.,$\mathcal{T}_k, \mathcal{R}_k, \forall k$) is known by all transmitters and receivers. A typical transmitter cooperation is enabled, where every transmitter is endowed the messages desired by its connected receivers, i.e., TXk has access to a subset of messages,$W_{\mathcal{R}_k}$ where $W_j, j \in \mathcal{R}_k$ denotes the message desired by RXj. We refer hereafter to this problem as

"TIM-CoMP" problem. We consider a block fading channel, where the channel coefficients stay constant during the coherence time. The network topology is fixed throughout the communication.

3.2.3 A Graph Theoretic Perspective

As a baseline, an interference avoidance approach (also known as orthogonal access) with the aid of selective graph coloring is first presented for the general topologies. The detailed proof and the outer bounds can be found in our journal paper [YG14].

- **Interference Avoidance via Graph coloring**

Before presenting the interference avoidance approach, we first introduce the following definition generalized from the standard graph coloring. Some basic graph theoretic definitions are recalled in Appendix A of our paper[YG14], which are also available in graph theory textbooks [WES01].

Definition(*Fractional Selective Chromatic Number*): Consider an undirected graph $\mathcal{G} = (\mathcal{V}, \mathcal{E})$ with a vertex partition $\mathbb{V} = \{\mathcal{V}_1, \mathcal{V}_2, \dots, \mathcal{V}_{\mathrm{p}}\}$ where $\cup_{\mathrm{i}=1}^{\mathrm{p}} \mathcal{V}_{\mathrm{i}} = \mathcal{V}$ and $\mathcal{V}_{\mathrm{i}} \cap \mathcal{V}_{\mathrm{j}} = \emptyset, \mathrm{i} \neq \mathrm{j}$. The portion $\mathcal{V}_{\mathrm{i}} (\mathrm{i} \in [\mathrm{p}] \triangleq \{1, \dots, \mathrm{p}\})$ is called a cluster. A graph with the partition $\mathbb{V}$ is said to be selectively n:m-colorable, if

(i) each cluster $\mathcal{V}_{\mathrm{i}}, \forall \mathrm{i}$ is assigned a set of m colors drawn from a palette of n colors, no matter which vertex in the cluster receives;

(ii) any two adjacent vertices have no colors in common.

Denote by $s\chi_{\mathrm{f}}(\mathcal{G}, \mathbb{V})$ the fractional selective chromatic number of selective n:m-coloring over a graph with the partition $\mathbb{V}$, defined as

$$s\chi_f(\mathcal{G}, \mathbb{V}) = \lim_{m \to \infty} \frac{s\chi_f(\mathcal{G}, \mathbb{V})}{m} \tag{3.18}$$

where $s\chi_f(\mathcal{G}, \mathbb{V})$ is the minimum *n* for the selective *n:m*-coloring associated with the partition $\mathbb{V}$.

Remark: If m=1, fractional selective graph coloring will be reduced to standard selective graph coloring (a.k.a. partition coloring) [DER14]. If $|\mathcal{V}_{\mathrm{i}}| = 1, \forall \mathrm{i} \in [\mathrm{p}]$, then fractional selective graph coloring will be reduced to standard fractional graph coloring [WES01].

Theorem*(TIM-CoMP DoF)*: For the TIM-CoMP problem with arbitrary network topologies, the symmetric DoF

$$d_{sym} = \frac{1}{s\chi_f(\mathcal{G}_e^2, \mathbb{V}_e)}, \mathcal{T}_i \subsetneq \mathcal{T}_j, and \;\; \mathcal{T}_j \subsetneq \mathcal{T}_{\mathrm{i}} \tag{3.19}$$

can be achieved by an interference avoidance approach built upon fractional selective graph coloring, where

$\mathcal{G}_{\mathrm{e}}$: the line graph of network topology $\mathcal{G}$, where the vertices in $\mathcal{G}_{\mathrm{e}}$are edges of $\mathcal{G}$;

$\mathbb{V}_{\mathrm{e}}$: a vertex partition of $\mathcal{G}_{\mathrm{e}}$, specifically vertices in $\mathcal{G}_{\mathrm{e}}$whose corresponding edges in $\mathcal{G}$have a common receiver form a cluster;

$\mathcal{G}_{\mathrm{e}}^2$: the square of$\mathcal{G}_{\mathrm{e}}$, in which any two vertices in $\mathcal{G}_{\mathrm{e}}$with distance no more than 2 are joint with an edge;

$s\chi_{\mathrm{f}}$: fractional selective chromatic number.

By connecting the achievable symmetric DoF of TIM-CoMP problem to fractional selective chromatic number, we are able to calculate the former by computing the latter with rich toolboxes developed in graph theory. The connection will be illustrated by the following example whose network topology was studied in [NA13] with no transmitter cooperation (message sharing).

- **An Example**

We focus for example on the network topology shown in Figure 3 and message sharing across transmitters is enabled. The optimal symmetric DoF is pessimistically 1/3 without message sharing. In contrast, if

transmitter cooperation is allowed, the symmetric DoF can be remarkably improved to 2/5 even with a simple interference avoidance scheme.

Without message sharing, the interference avoidance scheme consists in scheduling transmitters to avoid mutual interferences. In contrast, with message sharing, scheduling can be done across links rather than across transmitters. A possible link scheduling associated with Figure 3 is shown in Table 1. It can be found that each message is able to be independently delivered twice during five time slots, and hence symmetric DoF of 2/5 is achievable.

Table 1: Link scheduling

Slot	Scheduled Links (e_{ij}: TX-i→ RX-j)	Delivered Messages
A	e_{41}, e_{55}, e_{66}	W_1, W_5, W_6
B	e_{12}, e_{54}, e_{66}	W_2, W_4, W_6
C	e_{13}, e_{54}	W_3, W_4
D	e_{41}, e_{33}	W_1, W_3
E	e_{12}, e_{55}	W_2, W_5

Although the above link scheduling solution provides an achievable scheme for the example in Figure 3 the generalization is best undertaken by reinterpreting the link scheduling into a graph coloring problem, such that the rich graph theoretic toolboxes can be directly utilized to solve our problem. The nature of our problem calls for a distance-2 fractional clustered-graph coloring scheme, which consists of the following ingredients:

- Distance-2 fractional coloring: Both the adjacent links and the adjacency of the adjacent links (resp.edges with distance less than 2) should be scheduled in difference time slots (resp.assigned with different colors).
- Clustered-graph coloring: Only the total number of messages delivered by links with the common receiver (resp.colors assigned to the edges with the same vertex) matters. Thus, the number of assigned colors should be counted by clusters where the edges with common vertices are grouped together.

As such, the reinterpretation of the link scheduling as a distance-2 fractional graph coloring is shown in Figure 3.To ease presentation, we transform graph edge-coloring into graph vertex-coloring of the line graph. We first transform the topology graph $\mathcal{G}$ (left) into its line graph $\mathcal{G}_e$ (right) and map the links connected to each RX in $\mathcal{G}$ to the vertices in$\mathcal{G}_e$. For instance, the four links to RX-2 in G are mapped to Vertices 3,4,5,6 in $\mathcal{G}_e$. Then, we group relevant vertices in $\mathcal{G}_e$ as clusters, e.g., Vertices 3, 4, 5, 6 in $\mathcal{G}_e$ corresponding to the links to RX-2 are grouped as one cluster. By now, a clustered-graph is generated. The graph coloring can be performed as follows. For instance, if Vertex 2 in $\mathcal{G}_e$ receives a color indicated by 'A', Then Vertices 13 and 15 can receive the same color, because the distance between any two of them is no less than 2. Try any possible coloring assignment until we obtain a proper one, where each cluster receives m distinct colors out of total n ones, such that any two vertices with distance less than 2 receive distinct colors. There may exist many proper coloring assignments. The fractional chromatic refers to the minimum of n/m among all proper coloring assignments. In this example, we have m = 2 and n = 5. The vertices (i.e.,links in $\mathcal{G}$) with the same color can be scheduled in the same time slot. Accordingly, each cluster receivingtwo out of five colors means every message is scheduled twice during five time slots, yielding the symmetric DoF of 2/5. According to the connection between link scheduling and graph coloring, the inverse of the fractional chromatic number can serve as an inner bound of symmetric DoF of the general cellular networks, although its computation is NP-hard (Non-deterministic Polynomial-time hard).

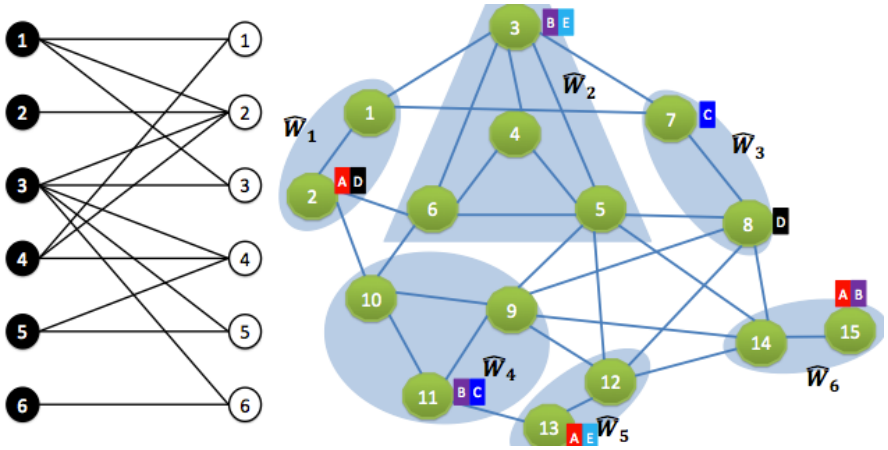

Figure 3: A topology of the 6-cell network.

3.2.4 An Interference Alignment Perspective

To gain further improvements, an interference alignment perspective is introduced with the alignment-feasible graph defined above, by which the sufficient conditions achieving a certain amount of symmetric DoF has been identified in our theorem. Further, by these conditions,we have identified the achievable symmetric DoF of regular networks. The detailed proofs and more results can be found in our journal paper [YG14].

- **Interference Alignment with Alignment-Feasible Graph**

In what follows, we introduce a new notion of alignment-feasible graph, which indicate respectively the feasibility of interference alignment for any two messages.

Definition (*Alignment-Feasible Graph*): The alignment-feasible graph (AFG), denoted by $\mathcal{G}_{\mathrm{AFG}}$, refers to a graph with vertices representing the messages and with edges between any two messages indicating if they are alignment-feasible. Two messages $W_i$and W_j are said to be alignment-feasible, denoted by $i \leftrightarrow j$, if

$$\mathcal{T}_i \subsetneq \mathcal{T}_j, \text{and} \quad \mathcal{T}_j \subsetneq \mathcal{T}_i \tag{3.20}$$

Remark: The previous condition implies the alignment feasibility, that is, it is feasible to align these two messages $W_i$and $W_j$in the same subspace without causing mutual interference by choosing proper sources of transmitting, such that the transmitted signal of one message will not interfere the intended receiver of the other message.

As such, given alignment-feasible condition, we are able to identify the sufficient conditions to achieve a certain amount of symmetric DoF as follows.

Theorem*(TIM-CoMP Symmetric DoF)*: For a *K*-cell TIM-CoMP problem with arbitrary topologies, the symmetric DoF

$$d_{\mathrm{sym}} = \frac{2}{\mathrm{K}} \tag{3.21}$$

are achievable, if there exists a Hamiltonian cycle or a perfect matching in $\mathcal{G}_{\mathrm{AFG}}$.

There is a very interesting observation. The alignment-feasible condition provided also implies the feasibility of selective graph coloring on $\mathcal{G}_e^2$. The fact that two messages satisfy the condition means there exist two vertices in two clusters i and j of $\mathcal{G}_e^2$ are not adjacent and hence can be assigned the same color. It follows that interference alignment is a general form of interference avoidance. Thus, interference alignment provides at least the same performance as interference avoidance. Even better, one advantage of interference alignment over interference avoidance is that, the number of dimensions of the subspace

to make interference alignment feasible could be less than the total number of colors (i.e., the total number of time slots to schedule links), as some subspaces may be absent at some receivers so as to decrease the number of required dimensions.

Specifically, by the above interference alignment approach, we could identify the achievable symmetric DoF of regular networks as follows.

For a (K,d) −regular network, the symmetric DoF

$$d_{\mathrm{sym}}(K,d)=\begin{cases}\frac{2}{\mathrm{d}+1},\mathrm{d}\leq \mathrm{K}-1\\ \frac{1}{\mathrm{K}},\mathrm{d}=\mathrm{K}\end{cases} \tag{3.22}$$

are achievable, when channel coherence time satisfies $\tau_c \geq d+1$.

In what follows, we present a detailed transmission scheme with interference alignmentfor an illustrative example.

- **An Example**

Let us consider the five-TX/RX pair regular network where each receiver is interfered by two other transmitters, as shown in Figure 4 By enabling transmitter cooperation, the symmetric DoF is improved from 2/5 to 1/2. In what follows, we will show an interference alignment scheme to achieve this.

For notational convenience, we denote by a, b, c, d, e the messages desired by five receivers, with the subscript distinguishing different symbols for the same receiver. We use multiple time slots to transmit these symbols, where multiple time slots span a space such that each symbol will be sent along with a specific direction spanned by vector V in this space. In this example, we use in total four time slots, and the symbols are sentalong with the directions spanned by five 4x1 random vectors $\mathrm{V}_1,\mathrm{V}_2,\mathrm{V}_3,\mathrm{V}_4\in\mathbb{C}^{4\times1}$, any four of which are linearly independent.The transmitted signals within four time slots are concatenated as

$$\mathbf{X_1}=\mathbf{V_1}\boldsymbol{c_1}+\mathbf{V_3}\boldsymbol{d_1},\mathbf{X_2}=\mathbf{V_2}\boldsymbol{d_2}+\mathbf{V_4}\boldsymbol{e_1} \tag{3.23}$$

$$\mathbf{X_3}=\mathbf{V_5}\boldsymbol{a_1}+\mathbf{V_3}\boldsymbol{e_2},\mathbf{X_4}=\mathbf{V_4}\boldsymbol{a_2}+\mathbf{V_1}\boldsymbol{b_2} \tag{3.24}$$

$$\mathbf{X_5}=\mathbf{V_5}\boldsymbol{b_1}+\mathbf{V_2}\boldsymbol{c_2} \tag{3.25}$$

where $\mathrm{X_i}\in\mathbb{C}^{4\times1}$ is the 4x1 vector from TX-i with j-th element being transmitted signal in j-th time slot. With sufficient coherence time (i.e., four time slots in this example), the received signal at RX-1 for example within four time slots can be written as

$$\mathbf{Y_1}=\sum_{i\in\mathcal{T}_1}\boldsymbol{h_{1,i}}\boldsymbol{X_i}+\boldsymbol{Z_1}\ =\boldsymbol{h_{1,1}}\boldsymbol{X_1}+\boldsymbol{h_{1,3}}\boldsymbol{X_3}+\boldsymbol{h_{1,4}}\boldsymbol{X_4}+\boldsymbol{Z_1} \tag{3.26}$$

$$=\boldsymbol{h_{1,3}}\boldsymbol{V_5}\boldsymbol{a_1}+\boldsymbol{h_{1,4}}\boldsymbol{V_4}\boldsymbol{a_2}+\boldsymbol{V_1}(\boldsymbol{h_{1,1}}\boldsymbol{c_1}+\boldsymbol{h_{1,4}}\boldsymbol{b_2})+\boldsymbol{V_3}(\boldsymbol{h_{1,1}}\boldsymbol{d_1}+\boldsymbol{h_{1,3}}\boldsymbol{e_2})+\boldsymbol{Z_1} \tag{3.27}$$

Recall that $\mathrm{V}_1,\mathrm{V}_2,\mathrm{V}_3,\mathrm{V}_4\in\mathbb{C}^{4\times1}$ are 4x1 linearly independent vectors spanning four-dimensional space, by which it follows that the interferences are aligned in the two-dimensional subspace spanned by $\mathrm{V}_1$and V_3, leaving two-dimensional interference-free subspace spanned by of V_4 and V_5 to the desired symbols $\mathrm{a}_1,\mathrm{a}_2$. Hence, the desired messages of RX1 can be successfully recovered, almost surely. Applying this to all other receivers, all receivers can decode two messages within four time slots, yielding the symmetric DoF of 1/2.

To illustrate the interference alignment, we describe the transmitted signals geometrically as shown in Figure 4. In this figure, we depict the subspace spanned by $\mathrm{V}_1,\mathrm{V}_2,\mathrm{V}_3,\mathrm{V}_4,\mathrm{V}_5$ as a four-dimensional space, where any four of them are sufficient to represent this space. We also denote the message for example $\mathrm{W_j}$ sent from TX i by $\mathrm{X_i(W_j)}$. Let us still take RX1 for example. Because of $\mathcal{T}_1=\{1,3,4\}$, the transmitted signals from the transmitters that do not belong to $\mathcal{T}_1$will not reach RX1, and hence the vector V_2 is disappeared. In addition, we have the interference-free signals in the directions of V_4 and V_5, and the aligned interferences carrying messages other than $\mathrm{a}_1,\mathrm{a}_2$ in the subspace spanned by V_1 and V_3. Recall that

vectors V_1, V_2, V_3, V_4 are linearly independent, almost surely. As such, the interference alignment is feasible at RX-1, and also it can be checked to be feasible at all other receivers.

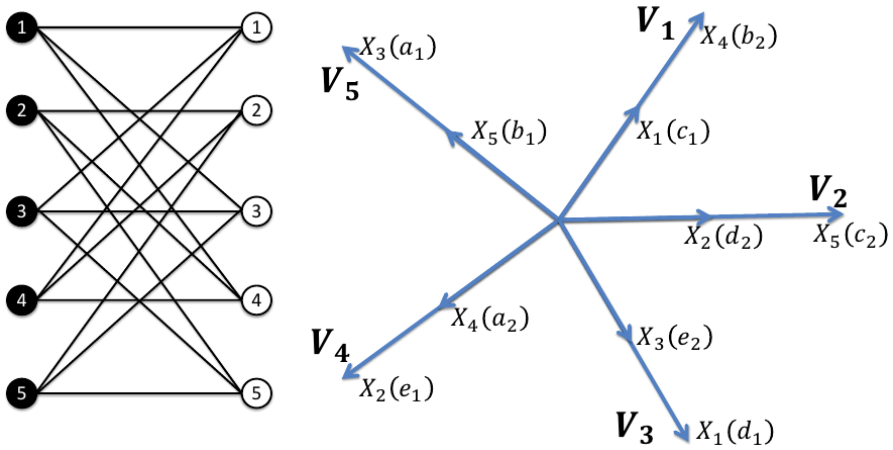

Figure 4:Illustration for a regular cellular network.

3.2.5 Conclusion

The topological interference management problem with transmitter cooperation, named TIM-CoMP problem, is considered from both interference avoidance and alignment perspectives. The achievable symmetric DoF is identified for a class of network topologies. Two illustrative examples are provided, by which the main interference management techniques, e.g., afractional graph coloring based interference avoidance and an interference alignment approaches, have been proposed, shedding light on how to generally exploit the benefits of both topological knowledge and transmitter cooperation. More results on larger classes of network topologies and the optimality can be found in our journal paper [YG14].

4 INTERFERENCE MANAGEMENT WITH REALISTIC CHANNEL MODELLING

4.1 Realistic Channel Modelling and Network Simulation

In deliverable D3.1 [D3.1, Section 5], we introduce a realistic simulation framework whose aim is to reduce the gap between real network performance and simulations using simplified models. Scenarios are proposed to tackle different network configurations and management techniques, and investigate the impact on radio network performances. The network setup, user traffic distribution and multi-cell multi-user 3D radio predictions compose together a reference evaluation framework that can be interfaced with third-party system-level simulators. It may be used (and customized) in the innovation WPs for simulation and assessment of HetNet deployment and algorithm performance in terms of service coverage, network capacity, energy efficiency and fairness.

In this deliverable, we present further results obtained for the case in which we consider only the macro-cell layer and develop possible interactions with partners. Figure 5 presents the macro-only network together with its main deployment parameters. This figure shows the macro-cells deployed on two rings (in orange and blue) around a central three-sector site (in red) with an average Inter-Site Distance (ISD) of 450 m. These are not located on real sites, but dominant locations have been selected that are representative of an operational network.

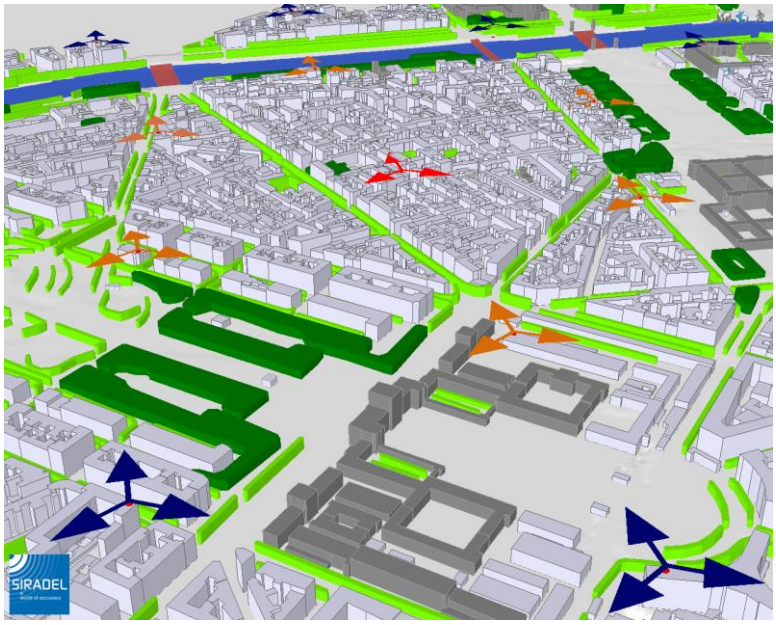

- Hexagonal site deployment: two rings around the central site, i.e. 19 sites corresponding to 57 cells (three cells per site).
- Average inter-site distance: 450 m.
- Average antenna height: 32 m above ground.
- Maximum total transmit power: 40 W per antenna.
- Antenna: directional, 14 dBi gain.
- Antenna electric down-tilt: 6°.

Figure 5: Macro-cell layer deployment in a real dense urban environment.

A square calculation zone of 1250 m side length and 5 m resolution is centred on the central macro site, representing UE locations at 1.5 m above ground. The path-loss from each eNodeB (eNB) to each UE location is computed with a highly efficient ray-based propagation model, Volcano [CL09] at a frequency of 2.6 GHz. The cell selection is assumed to be based on the best DL received power from each cell. Figure 6on the left displays the best server map, showing in distinguishable colours the index of the selected cell at each UE location. On the right of Figure 6, the resulting received power after cell selection is shown.

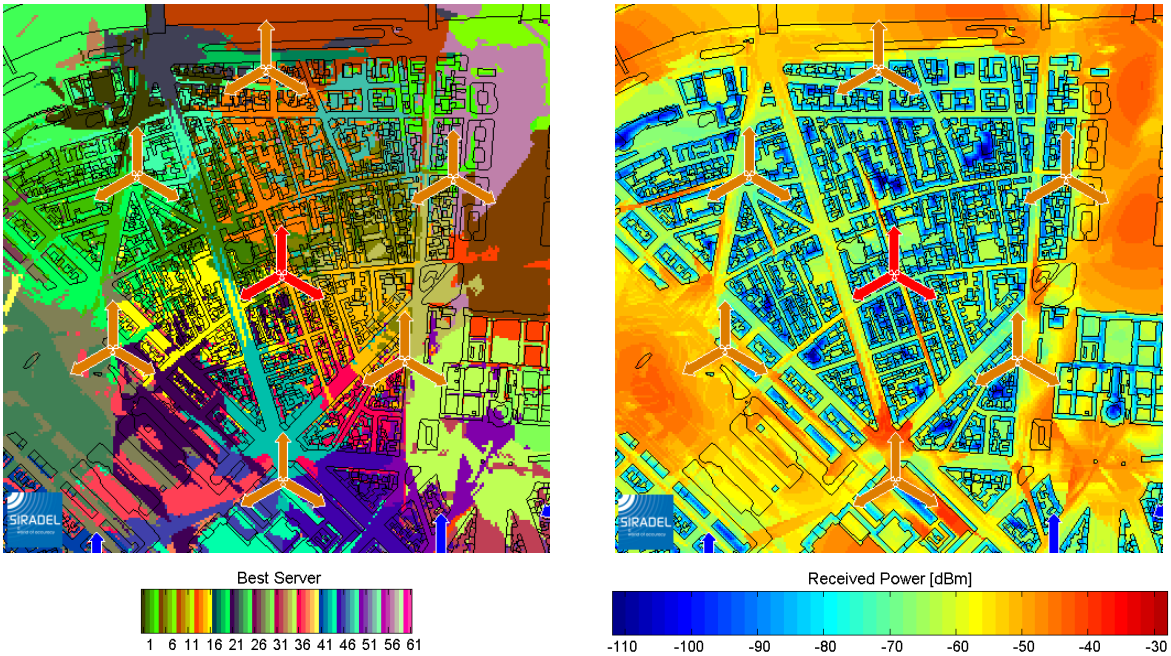

Figure 6: Cell selection (left) and received power from selected cell (right).

The best server map and the path-loss results can be combined to compute the interference from the non-serving cell on the DL at each UE location. The calculation relies on a simple abstraction of Orthogonal Frequency Division Multiple Access (OFDMA) Media Access Control (MAC) layer protocols without any interference mitigation technique: the allocation of resource blocks is uniformly distributed in time and frequency domains, and performed independently in each cell. The average interference level in a given Resource Element (RE) coming from a non-serving cell thus depends on the received power from this cell and the likelihood that the same RE is used by this cell. This probability is directly linked to the traffic load of the considered interfering cell, which ranges from 0 to 100%. The total interference level in W is finally given by:

$$I = \sum_{i \neq j} EPRE_i . TL_i . PL_i \qquad (4.28)$$

where:

- i is the index of the interfering cell,
- j is the index of the serving cell,
- EPREi is the Energy Per Resource Element of interfering cell i, in W,
- TLi is the traffic load of interfering cell I,
- PLi is the path-loss between interfering eNBi and the UE, including antenna radiation gain.

Figure 7 is the resulting DL interference map obtained for a typical 10 MHz bandwidth and 50% traffic load for all cells; a single antenna is used both at the eNB and the UE. We observe strong interference levels in large open areas which are covered without obstruction by multiple eNBs. This interference map is the basis of other post-processing aiming at assessing the network performance. In deliverable D3.2 [D3.2, Section 4], we evaluate the impact of beamforming on Signal to Interference plus Noise Ratio (SINR) and mean user peak throughput. In deliverable D4.2 [D4.2, Section 3.6], we add the small-cell layer and refine the interference calculation to take into account the cell range extension bias and the almost-blank sub-frame duty cycle. Several quality of service metrics are assessed under different small-cell deployment strategies. The interference map may also be refined with more precise RRM algorithms.

The 'Joint Location and Interference Prediction for ICIC' innovation described in the following section can actually take advantage of the deterministic path-loss maps to predict more realistic interference maps.

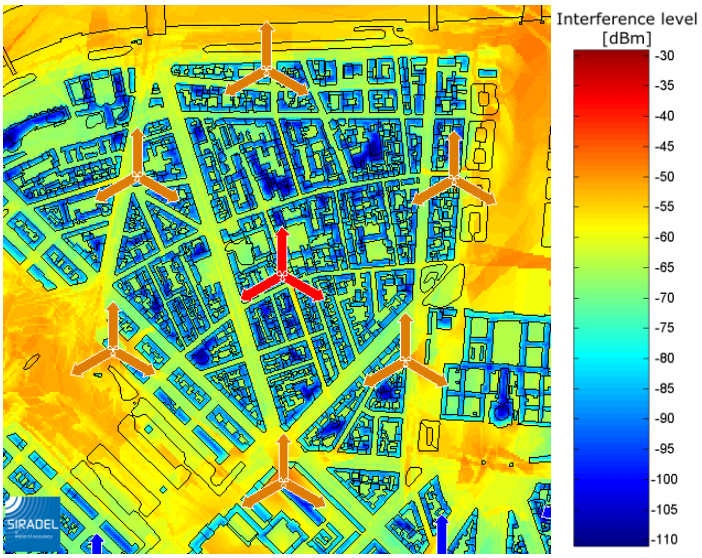

Figure 7: Interference map.

4.2 Joint Location and Interference Prediction for ICIC

To meet the constant growth of traffic, the 3GPP LTE-Advanced (LTE-A) and beyond explores ways to extend LTE technology in order to reach very high data rates (i.e., on the order of 1 Gbps) and high spectral efficiency (i.e., 30 b/s/Hz and 2.6 b/s/Hz as peak and average values, respectively). However some of the proposed techniques, such as Massive MIMO [LET14] and Non-orthogonal multiple access [OIS12] are complex and significant research efforts are still needed to bring the latter solutions to reality. In the meantime, a straightforward but extremely effective way to increase the network capacity is to make the cells smaller and keep the network closer to the user. Thus future wireless networks are becoming more and more heterogeneous, as we move towards 5G. Heterogeneous networks (HetNets) are deployed according to the non-uniform users' distribution, in the sense they are constructed with layers of macro and small cells, and accommodate other technologies e.g. Wi-Fi. Since the inter-cell interference (ICI) level suffered by users in downlink depends on the relative positions of mobile users and the fixed elements of infrastructure, an increase of cell densification implies an increase of cell edge users suffering from a high ICI level. Several techniques of Inter-Cell Interference Coordination (ICIC) and/or Cancellation have been proposed in the literature to mitigate the interference level and improve the users SINR in heterogeneous networks such as, the frequency domain ICIC using the Soft Frequency Reuse technique [BPG10] [GBG11] and the time domain ICIC based on the Almost Blank Subframes [DMM14].

In order to use the time and/or frequency domain ICIC, users are classified into two sets: small cell users and macro cell users. This classification is based on the users long-term SINRs w.r.t. the different base stations which depends on their location. Thus, the ICI Coordination/Cancellation techniques may take advantage of external (and most often static) information such as location and average interference levels. On the other hand, to fully exploit the LTE-A network capacity, the major challenge of standard communication in such environments is to provide a good spectral efficiency and fairness among users, even for cell edge users, by adopting an adequate Radio Resource Management (RRM) policy and flexibility between the cells in terms of cell size fluctuation (e.g. cell zooming techniques [ZKZ13]).

The capability to properly manage the inter-cell interference, to manage and allocate time/frequency resources, to offload the data traffic, to define optimal packet relaying strategies, or to optimize the

transmission parameters, is clearly conditioned on the actual levels of interference suffered by the users whatever their location. Then a way to perform this optimization is to provide these systems with information about the instantaneous ICI level at each pixel of the area of interest.

Our goal is to propose a joint location and interference prediction in order to assist subsequent location-based ICIC mechanisms, and enable better in-site dynamic spectrum access. The temporal aspect of the joint location and interference prediction could be exploited for instance in issues such as radio resource allocation, traffic offload and handovers decisions. Thus, in the frame of this study, we aim at estimating the inter-cell interference level suffered by users in the downlink of a heterogeneous network, according to their locations. The main idea is to create a 2D interference map. A third dimension representing time will be incorporated to the interference map where users' tracking mechanism and interference time varying prediction will be considered. The proposed spatio-temporal interference map scheme is illustrated in Figure 8. For more details about the proposed method and the main steps to build the spatio-temporal interference map, please refer to [D3.1, Section 4.4]. .

As a first step we have to build a 2D interference map. Such maps have already been mentioned in the recent literature. However the optimal and most practical way to build them is still an open issue. A state of the art was presented in the previous deliverable [D3.1, Sections 4.4.1 – 4.4.3]. The investigated methods were classified in three types: statistical interference estimation, deterministic interference map, and interference map based on low resolution fingerprint. In our work, we focus on the statistical type which is essential for the interference map initialization especially when starting from scratch. The interference map obtained with such methods is universal and can be applied without a priori information about the area infrastructure. In addition, the statistical interference estimation is able to take into account different network configurations e.g. the networks' activity rate which is essential when heterogeneous networks are considered.

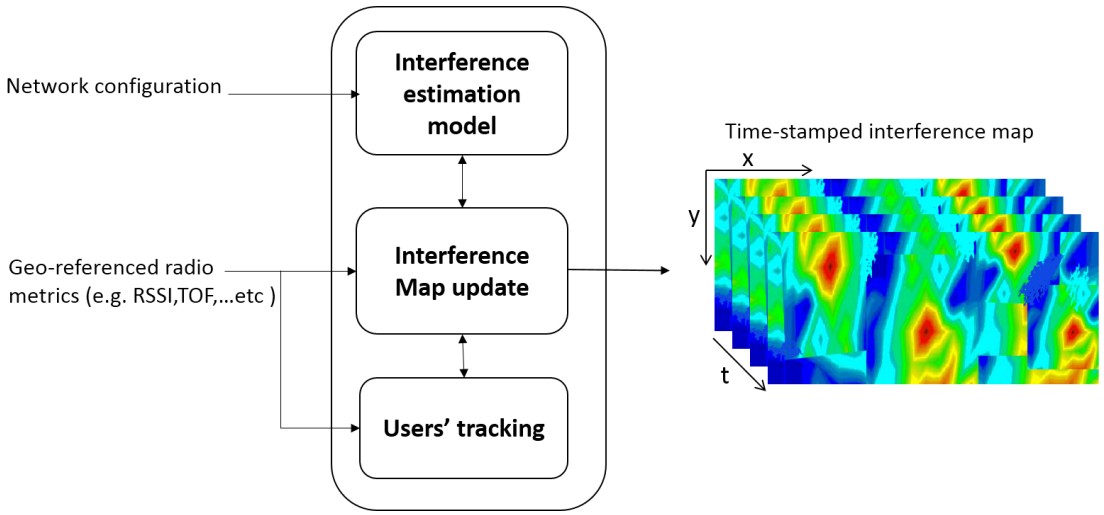

Figure 8: Space/time interference prediction.

The statistical characterization of inter-cell interference level has been investigated for a long time, under different scenarios, and following several approaches. Both regular networks (i.e., BSs position following a hexagonal grid) and random networks (i.e., BSs positions modeled with a Poisson Point Process (PPP)) were investigated. In practical deployment, BSs positions do not follow an hexagonal grid. Figure 9 illustrates the inter-cell interference Cumulative Distribution Function (CDF) obtained in both regular and random networks, assuming identical BSs densities. It is noticeable that the ICI distributions obtained in both cases are not similar. With the study carried out in [GWC13] which compares the SINR CDF curves obtained in the two deployments with the one obtained in a realistic environment, the accuracy of the stochastic geometry approach has been proved once again: the SINR CDF obtained in a random network is closer to the realistic SINR CDF than the one obtained in a regular network. Indeed, the random network model copes with the heterogeneous network complexity, especially for the small cells configuration (e.g. small cells sleep mode). Thus, in this work, the stochastic geometry approach is considered. Its flexibility

and a large arsenal of mathematical tools can lead to a closed form of the inter-cell interference estimation analytical model.

4.2.1 Statistical interference estimation state of the art – Stochastic approach

The stochastic approach has been widely considered in the literature, especially to enable in-depth theoretical analysis in K-tier heterogeneous networks. In [DGB12] for instance, the authors derive the expression of the coverage probability, average rate achieved by a randomly located user and average load of each tier's BS. In [WG14], considering Rayleigh fading only, the DL interference in K-tier HetNets is estimated based on the moment generating function. The authors have subsequently extended their study in order to estimate the wireless activity according to the measured interference level power in [WG13]. Downlink interference statistics are also derived in [BHA11], where the cumulants of the interference are given for random punctured PPP, assuming that the latter keeps its Poisson properties. The cumulants expression derivation requires the joint statistics of the distance between the transmitters and the receivers. Both the case of a unique transmitter and the case of multiple transmitters were investigated. One step further: a mobility model is considered in [GH14] in order to derive the expectation value of the interference. However, all these studies have in common to consider only the fast fading effects, modelled by Rayleigh or Nakagami-m distributions.

To the best of our knowledge, when stochastic geometry is applied, only few works take into accountlog-normal shadowing for modelling the networks statistics.They thus neglectits significant impact on the user's received signal strength. This is mainly due to the high complexity of the mathematical analysis and the inability to derive closed forms since there does not exist any generic expression for the Probability Distribution Function (PDF) of a sum of lognormal random variables. So as to derive an analytical upper bound for the dimensioning outage probability respectively in Uplink (UL) or DL LTE networks, the authors of [KMD13] and [DFM09] consider shadowing as a mark of the PPP. To characterize the UL interference profile experienced by autonomous self-organizing femto cells, modelled with a Binomial Point Process (BPP), the authors in [LBC10] use a Gauss-Hermit polynomial function [PT04] to approximate the moment generating function of the lognormal shadowing. Using the same approximation technique and considering PPPs, the cumulants of downlink co-channel interference are derived in [LBL13] for a self-organizing network with biased cell association and interference coordination.

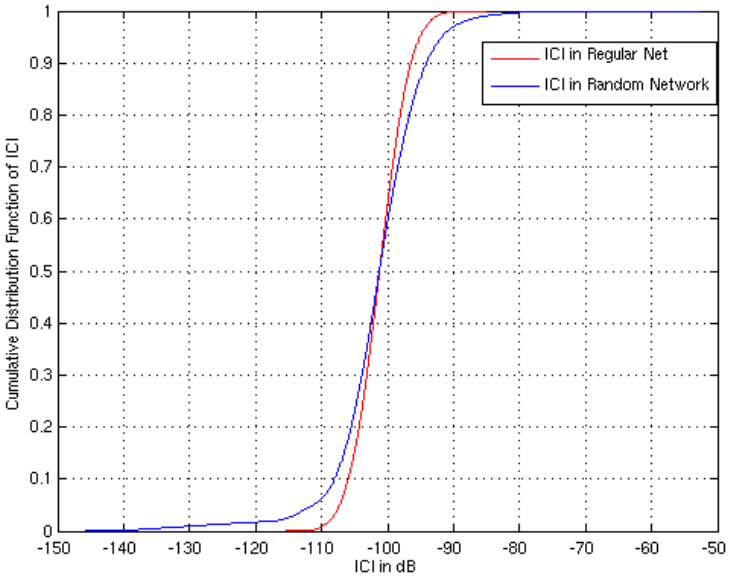

Figure 9: Cumulative distribution function of inter-cell interference level in regular and random network.

In [DA13], based on the Signal to Interference Ratio (SIR) expression, the downlink rate distribution expression is derived under a generalized cell selection model. In their analysis, the shadowing is considered as a transformation of each location where the SIR distribution is derived by applying the

displacement theorem [BB09] as detailed in the Lemma below to the SIR distribution derived in [JSX12] in case of Rayleigh fading effects only. After defining the Path Loss Process with Shadowing (PLPS), authors of [ZH14] derive the coverage probability expression for inter-cell interference coordination and intra-cell diversity networks, where the fading coefficient and the scheduling decision are considered as a mark of the PLPS. The authors of[HKB12] opted for approximating the product of the fast fading and the shadowing coefficients with a gamma distribution by modelling the Rayleigh fast fading with a gamma distribution of both shape and scale equal to 1 (i.e., Γ(1,1)). Based on this approximation, the Laplace transform of the interference in Heterogeneous network is derived.

Relying in part on some of the previous results and intermediary derivations (and more particularly, on works carried out in[WG14] and [DA13]), our goal herein is to develop a new analytical model for location-dependent DL ICI estimation in K-tier HetNets, that takes into account the radio environment propagation and especially the shadowing impact. The model only assumes (as inputs) that:

- The UE position is a priori known (e.g., pre-positioned in a real system through GPS and/or any terrestrial wireless means).
- The BS density, path loss model including shadowing standard deviation are known a priori.

Since the aggregate inter-cell interference depend on the frequency allocation, both separate frequency allocation and co-channel deployment are investigated. The following section presents the considered scenario and the main assumptions.

4.2.2 Considered assumptions and scenario

In our study, we focus on inter-cell interference in K-tier heterogeneous network, modeled with a superposition of K independent homogeneous Poisson point processes $\Phi_k = \{x_{1,k}, x_{2,k}, \dots, x_{1,K}\}$ of intensity λ_k, where $k = 1, \dots, K$, and $x_{i,K}$ denote the 2 dimensional K-th tier BSs coordinates. Figure 10 shows a realization of a two-tier heterogeneous network, composed of macro BSs (blue triangles) distributed according to a homogeneous PPP of intensity λ_m and small BSs (red circles) distributed with a homogeneous PPP of intensity λ_s.

LTE-A standard compliant scenario is considered where OFDMA technique is used for resource allocation. Thereby, intra-cell interference is cancelled and the total interference received by a user u on the downlink is caused only by the nodes transmitting on the same frequency band. However the macro and small cell base stations (e.g., micro, pico, femto cells) can be allowed to transmit in:

1. the same frequency band, which is known also as a co-channel deployment: in this case, the users are interfered by all the network nodes without distinction between tiers and the aggregate interference is called a ***co-channel interference***.
2. separate frequency bands,in which case the inter-cell interference is called a ***co-tier interference***, where the interference is generated between network elements on/belonging to the same layer. The macro cell users and the small cell users are interfered only by the macro cell base stations and the small cell base stations, respectively.

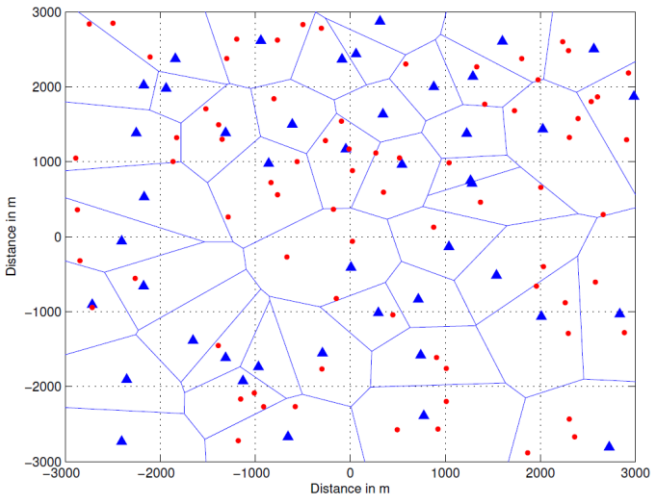

Figure 10:Two-tier heterogeneous network realization: Both macro (blue triangles) and small (red circles) BSs are distributed as independent PPPs with$\lambda_{m=}2\lambda_s$.

The analytical model of location-based ICI is derived in both cases of deployment and considering various sources of channel variations.

First, a standard path loss function that depends on the distance $r_{i,k} = \| x_{i,k} \|$ between the user and the interfering base station *i* is used. The path loss function is classically expressed by:

$$Pl(r_{i,k}) = l \; r_{i,k}^{\;-\gamma} \tag{4.29}$$

where, l and $\gamma > 2$ are respectively, the constant path loss and the path loss exponent. Their values depend on the considered scenario (i.e., macro or small cell scenario), and can be instanced by using the corresponding models specified in [E-UTRA10].

In addition, Rayleigh fast fading effect is taken into account by a path loss multiplicative factor h_i that follows an exponential law $h \sim \exp(1)$.

In [KVP12] it has been shown that the shadowing has a considerable impact on the ICI level. Thus, in our study a lognormal shadowing $\chi = 10^{z/10}$, such that $z \sim N(\mu, \sigma)$ is considered μ and $\sigma$are, respectively, the shadowing mean and standard deviation in dB. We denote as$\mu_k$and σ_k the specific shadowing parameters associated with the k[th] tier. Actually, such shadowing leads to a non-closed form of both the channel model and the ICI expression. That is the main reason why, following the same approach as in [DA13] and [KBK13] we include the shadowing in the path loss computation as:

$$Pl(\chi_{i,k}, r_{i,k}) = l(\chi_{i,k}^{-\frac{1}{\gamma}} r_{i,k})^{-\gamma} \tag{4.30}$$

This is possible through the displacement theorem [BB09]. Considering the shadowing as a random displacement of the base stations locations, the following lemma is derived.

Lemma: *Let* $\Phi = \{x_1, x_2, \ldots\} \in \mathbb{R}^2$ *be a homogeneous PPP of intensity* λ *. If each point* x_i *is transformed as* $y_i \in \mathbb{R}^2$ *such that* $y_i = \chi_i^{-1/\gamma} x_i$, *where the variables* χ_i *are independent and identically distributed (i.i.d) and* $E(\chi_i^{2/\gamma}) < \infty$, *where E denotes expectation, the resulting point process* $\Phi^{(e)} = \{y_1, y_2, \ldots\}$ *is also a homogeneous PPP with intensity* $\lambda^{(e)} = \lambda \; E[\chi_i^{2/\gamma}]$.

According to Lemma, the new Process $\Phi_k^{(e)}$, defined by the transformed location of equation (4.30), is also a homogeneous PPP whose intensity $\lambda_k^{(e)}$ depends on the intensity λ_k of the original PPP and on $E[\chi_k^{2/\gamma}]$ the fractional moment of the shadowing (dropping the index i by abuse of notation). This method can be used for any general distribution of χ_k as long as $E[\chi_k^{2/\gamma}] < \infty$. In case of a lognormal distribution, the fractional moment is $E[\chi^{2/\gamma}] = \exp\left(\frac{\ln 10}{5}\frac{\mu_k}{\gamma} + \frac{1}{2}\left(\frac{\ln 10}{5}\frac{\sigma_k}{\gamma}\right)^2\right)$ [DA13]. It is noticeable that $E[\chi_k^{2/\gamma}] < \infty$ when both μ_k and σ_k are finite.

Based on these radio environment parameters, a location-dependent DL ICI level analytical model is derived in the next section.

4.2.3 Location-dependent inter-cell interference estimation

The downlink inter-cell interference incurred by each user is computed as the total received power from the neighboring nodes transmitting in the same frequency band. It depends on the deployment type. Thus, in the next subsections, analytical models are derived for both co-tier and co-channel interference cases. Due to the path loss, the interfering signal strength mainly depends on the distance between the interfered user and the interfering node. At large scale (i.e., r_i>>1) the interfering signal strength becomes negligible. In order to derive the location-dependent inter-cell interference level expression, we limit the zone of observation to a ring area around the user, inscribed between two circular areasrespectively of radius R_{ob} (i.e., the radius of the observation zone) and *r* (i.e. the minimum distance between the user and the interfering BSs), as shown in Figure 11. Without loss of generality, the downlink analysis is performed at a typical user assumed to be located at the origin [BB09].

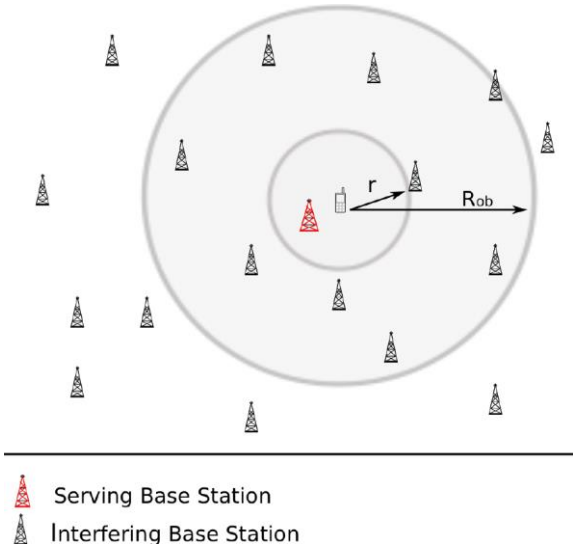

Figure 11:Observation zone containing the more interfering BSs. Rob is the observation zone radius. r is the minimum user-interfering BS distance.

a- Co-tier interference estimation

In a separate frequency deployment, the user u is interfered only by the neighboring BSs of the same tier i.e., the BSs located at $x_{i,k}$ where $x_{i,k} \in \Phi_k$ except b_s the serving BS. BSs transmit power is denoted by P_k, assumed to be constant for each tier. For the sake of simplicity, we note in this subsection the

transmission power as P, and drop the index k for all variables, since the analysis concerns only one tier. The total co-tier interference is then:

$$I_t = \sum_{i \in \Phi_k,\, i \neq b_s} P\, h_i\, l\, (\chi_i^{-1/\gamma} r_i)^{-\gamma} \tag{4.31}$$

Since there is no known expression for the PDF of the inter-cell interference, the Moment Generating Function (MGF) is used to characterize it:

$$MGF(I_t) = E\left[\exp(-s\, I_t)\right] = \underset{\Phi_k^{(e)}}{E}\{\underset{g_i}{E}(\exp(-s \sum_{i \in \Phi_k^{(e)}, i \neq b_s} g_i y_i^{-\gamma}))\} = \underset{\Phi_k^{(e)}}{E} \prod_{i \in \Phi_k^{(e)}, i \neq b_s} \underset{g_i}{E}(\exp((-s y_i^{-\gamma} g_i))$$

$$\overset{(a)}{=} \underset{\Phi_k^{(e)}}{E}\left\{\prod_{i \in \Phi_k^{(e)}, i \neq b_s}\left(\frac{\eta}{\eta + s\, y_i^{-\gamma}}\right)\right\} \overset{(b)}{=} \exp\left\{-2\pi\lambda_k^{(e)} \int_r^{R_{ob}}\left(\frac{1}{1+u^{\gamma/2}}\, du\right)\right\} = \exp\left(-\pi\lambda_k^{(e)} (s/\eta)^{2/\gamma}\, \Psi(r, R_{ob}, \gamma)\right)$$

where $g_i = P\, l\, h_i$, which impliesthat the random variable g_i follows an exponential distribution of parameter $\eta = \frac{1}{P\, l}$. $y_i = \chi_i^{-1/\gamma}\ r_i$ are the transformed locations.

(a) is obtained with the moment generating function of the exponential variable. Similarly, (b) results from the expression of the moment generation function of a PPP given in [SKM87]and of an integration by substitution considering $u^{\gamma/2} = (\frac{\eta}{s} r^{\gamma})$.

For $\gamma = 4$, we obtain

$$\Psi = \int_r^{R_{ob}} \frac{1}{1+u^2}\, du = \arctan(R_{ob}) - \arctan(r) \tag{4.32}$$

The PDF $f_{I_T}(I_t)$ of the co-tier interference can be easily derived by computing the inverse Laplace transform of the MGF as:

$$f_{I_T}(I_t) = \mathsf{L}^{-1}\left[MGF(I_t)\right] = \mathsf{L}^{-1}\left[\exp\left(-\pi\lambda_k^{(e)}\, s/\eta^{2/\gamma} \Psi(r, R_{ob}, \gamma)\right)\right] \tag{4.33}$$

Hence, the PDF of I_t is expressed as[AS64]:

$$f_{\mathsf{I}_T}(\mathsf{I}_t) = \frac{\sqrt{\pi}\lambda_k^{(e)} \sqrt{1/\eta}\, \Psi(r, R_{ob}, \gamma)}{2 I_t^{3/2}} \cdot \exp\left(\frac{-(\pi\lambda_k^{(e)}\, \Psi(r, R_{ob}, \gamma))^2}{4\eta\, I_t}\right) \tag{4.34}$$

and the Cumulative Distribution Function (CDF) is derived accordingly as:

$$F_{\mathsf{I}_T}(\zeta, \gamma) = \int_0^{\zeta} f_{\mathsf{I}_T}(\mathsf{I}_t, \gamma) dI_t = \mathrm{erfc}\left[\frac{\pi\lambda_k^{(e)}\, \Psi(r, R_{ob}, \gamma)}{2\sqrt{\eta\zeta}}\right] \tag{4.35}$$

In order to build the interference map, we choose the median value of the co-tier interference (i.e., an arbitrary quantile $\zeta = 0.5$). The performed analysis is still valid for any arbitrary a priori quantile. Thus, the median value is expressed as:

$$\mathsf{M}_{\mathsf{I}_t} = \left(\frac{\pi\lambda_k^{(e)}\, \Psi(r, R_{ob}, \gamma)}{2\sqrt{\eta}\, \mathrm{erfc}^{-1}(0.5)}\right)^2 \tag{4.36}$$

One can notice that the analytical model of the co-tier interference median value is given as a function of r the minimum distance between the user and the interfering BS, which depends on the user's location, assumed known.

b- Co-channel interference estimation

In co-channel deployment, the user u is interfered by all the BSs transmitting in the same frequency band. In fact, the global point process that models the K-tier HetNets is a superposition of K independent homogeneous PPP. Let $\varphi = \cup \varphi_k, k = 1,2,\ldots,K$, where φ_k models the k^{th} tier homogeneous PPP of intensity λ_k and P_k the transmission power with which each tier contributes to the aggregate co-channel interference. *When an open access is considered i.e., when the user can connect to a BS from each tier*, the resulting overall co-channel interference is equivalent to the sum of the co-tier interference terms computed for each tier, and can be expressed as:

$$I_c = \sum_{k=1}^{K} \sum_{i_k \in \Phi_k, i_k \neq b_s} P_k h_{i_k} \, l(\chi_{i_k}^{-1/\gamma} r_{i_k})^{-\gamma} \tag{4.37}$$

The same assumptions in terms of network configuration as those used in the previousdeployment are thus considered. We define $G_k \sim \exp(\eta_k)$ a random variable that corresponds to each tier k, where $\eta_k = \frac{1}{l\, P_k}$. The same steps as the ones used in a co-tier interference PDF derivation are performed.

For a K-tier network, we define $\varphi = \cup \varphi_k, k = 1,\ldots,K$.

The MGF of the co-channel interference is:

$$MGF(I_C) = \mathsf{E}_{\Phi^{(e)}}\{\mathsf{E}_{G_k}[\exp(-s\, I_c)]\} = \prod_{k=1}^{K} \exp\{-\pi \lambda_k^{(e)} (\frac{s}{\eta_k})^{\frac{2}{\gamma}} \Psi(r_m, R_{ob}, \gamma)\} \tag{4.38}$$

The PDF of I_c is expressed as:

$$f_{I_C}(I_c) = \frac{\sqrt{\pi}\, \Psi(r_m, R_{ob}, \gamma)}{2\, I_c^{\frac{3}{2}}} \sum_{k=1}^{K} \frac{\lambda_k^{(e)}}{\sqrt{\eta_k}} \exp\left\{ - \frac{(\pi\, \Psi(r_m, R_{ob}, \gamma))^2}{I_c} \sum_{k=1}^{K} \frac{\lambda_k^2}{4\eta_k} \right\} \tag{4.39}$$

where $r_m = \min\{r_k\}, \forall r_k \in \Phi_k$, is the minimum distance between the user and the interfering BS without distinction regardless of its belonging tier.

Hence, the CDF is:

$$F_{\mathsf{I}_C}(\zeta, 4) = \mathrm{erfc}\left[\frac{\pi\, \Psi(r_m, R_{ob}, 4)}{2\sqrt{\zeta}} \sum_{k=1}^{K} \frac{\lambda_k^{(e)}}{\sqrt{\eta_k}} \right] \tag{4.40}$$

Similarly to the previous subsection, to obtain the interference map in a co-channel deployment, an arbitrary quantile $\zeta = 0.5$ is used. The median value of the co-channel interference $\mathsf{M}_{\mathsf{I}_c}$ is then:

$$\mathsf{M}_{\mathsf{I}_c} = \left[\frac{\pi\, \Psi(r_m, R_{ob}, 4)}{2\, \mathrm{erfc}^{-1}(0.5)} \sum_{k=1}^{K} \frac{\lambda_k^{(e)}}{\sqrt{(\eta_k)}} \right]^2 \tag{4.41}$$

The value of $\mathsf{M}_{\mathsf{I}_c}$ given in Equation (4.41) is an immediate consequence of Equation (4.40).

4.2.4 Location-dependent ICI mapping performance evaluation

For performance analysis, we consider a two-tier LTE HetNet e.g., macro and micro cell, operating at a carrier frequency f_c of 2.6 GHz. The macro base stations are modeled with a homogeneous PPP of intensity $\lambda_m = 5.10^{-6}$ BS/m^2. The number of deployed small cell is obviously higher, then we model them

with a homogeneous PPP of intensity $\lambda_s = 2\lambda_m$. The resulting HetNet is then a superposition of the two PPPs. We assume that the macro base station transmission power is set to $P_1 = P_m = 43\,\mathrm{dBm}$ whereas, the transmission power of the small cell BSs is set to $P_2 = P_s = 33\,\mathrm{dBm}$ [3GPP1]. The interfering base stations are considered to be in Non-Line Of Sight (NLOS), thus the NLOS Urban Macro (UMa) propagation model is considered for the path loss computation of macro BSs and the Urban Micro (UMi) path loss model for the small cell BSs [E-UTRA10]. The lognormal shadowing is considered centered (i.e., $\mu_k = 0$) with a standard deviation σ_k of 6 dB and 3 dB in macro and micro cell scenarios, respectively.

Figure 12shows the co-tier interference map in a macro cell scenario, obtained with the corresponding analytical model derived in the previous section. With the colormap, we notice that the the co-tier interference median value as given by the above analytical method overall reflects the inter-cell interference behavior. When the distance between the user and the interfering base station gets smaller, the median value of the co-tier interference is higher, as expected. The cell edge users are exposed to a high interference level, except when the interfering base stations are farther, due to the large cell size.

In order to study the reliability and the validity of the underlying analytical model, our inter-cell interference map is compared to a realistic ICI map obtained through simulations, following a brute force method, where the snapshot ICI level is computed over all the possible user's locations in the area on interest, depending on the network node positions. Without loss of generality, the numerical results presented in this section are obtained in case of a separate frequency band allocation and the analytical performance analysis is only related to the co-tier interference. The same conclusions are obtained in case of co-channel interference analytical model.

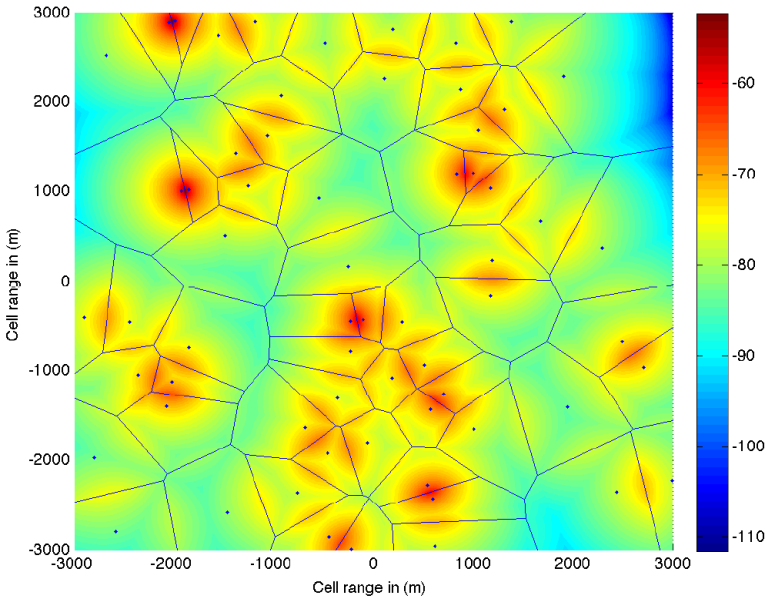

Figure 12:Co-tier Interference map in Macro cell scenario.

For a given deployment shown in Figure 13 left, an analytical co-tier interference map (i.e., based on our median model) and a realistic simulation-based map (thus reflecting the actual instantaneous interference level suffered by the UE) of a central cell (presented with a red BS) are illustrated in Figure 13 middle and right, respectively. The color code represents the co-tier interference level.

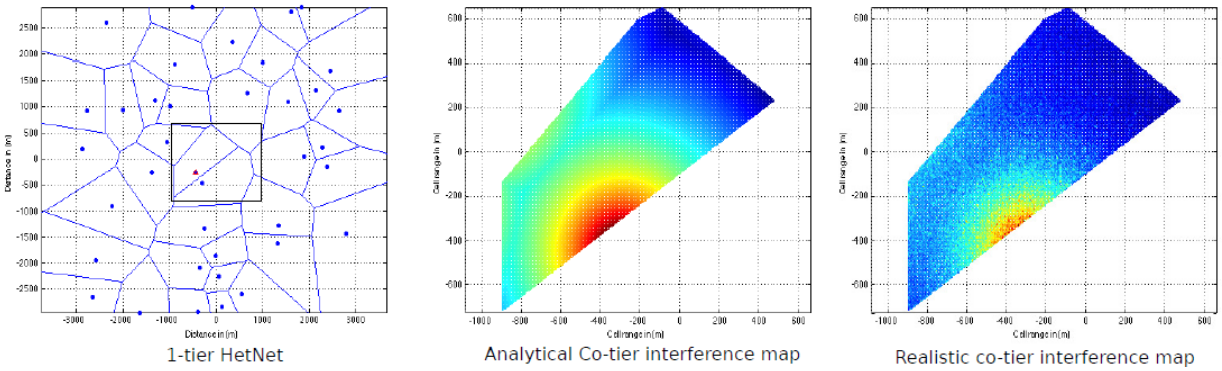

Figure 13:Co-tier analytical and simulated maps.

The co-tier interference level obtained with the analytical model is smoothed. The value varies according to the distance from the interfering BSs. When comparing to the realistic case, it is noticeable that the the analytical model overestimates co-tier interference level in areas close to the strongest interfering BS.

To identify these areas, the relative error between the analytical co-tier interference median value and the realistic co-tier interference is illustrated according to the user's location inFigure 14. We notice that, in most cases (i.e. 70% of the tested locations), the proposed analytical model overestimates the co-tier interference level with a relative error less than 5 percentile (which corresponds to 2 dB absolute error). The large difference between the realistic co-tier interference and the analytical prediction concerns the area close to the strongest BS.. In fact, with the analytical prediction, the co-tier interference level degrades slowly as a function of the distance r, which means that the areas where users suffer from high theoretical ICI level are extended.

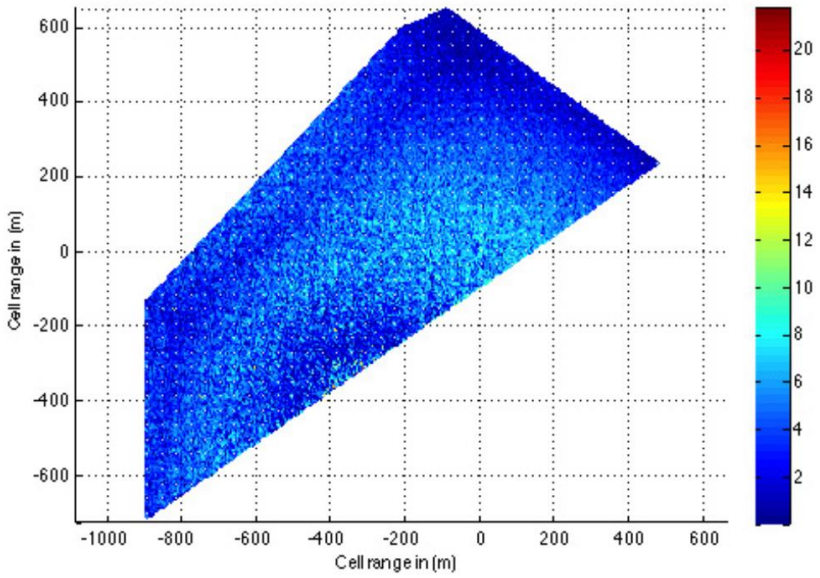

Figure 14: Relative co-tier interference error in (%).

4.2.5 Conclusion and future work

The interest of the proposed location-dependent ICI estimation model lies in its low computational complexity (making implementation practical for embedded predictions) and its simplicity with respect to the required input parameters (i.e., small amount of required a priori information). The proposed model indeed needs the followinginputs: i) information about the network configuration (i.e., the BS density and the shadowing standard deviation) that can be defined according to the studied area (e.g., dense urban, urban, rural, etc.) and ii) the user's location that can be obtained by GPS (in outdoor), which nowadays

most smartphones are equipped with, or relying on various methods such as fingerprinting, trilateration, triangulation, tracking filters, message-passing, etc.

Hence, such a model will be applied as an initialization of the spatio-temporal interference map, when starting from scratch. The coarse statistical model will be refined and updated iteratively, according to the geo-referenced metrics collected in the locations physically visited by the mobile terminals, in a self-learning step. As an example, in relevant approaches from the recent state of the art, most of them exploit the RSS measured by users moving around in the area. In our case, this metric can be exploited in order to refine the interference map.

Then, user tracking will be performed using the user's location information, the collected radiolocation metrics and their a priori mobility models. Using jointly the interference map and the UEs' tracking process, the inter-cell interference suffered by users at the location visited in the next Transmission Time Interval (TTI) will be estimated. This inter-cell interference level will be considered as an input to the location-based ICIC mechanisms.

Up to now, we have assumed that the user's location is known. In future work, we will consider an uncertainty of the estimated positions (mobile users and fixed elements) and will evaluate the performances of the proposed analytical model accordingly. Afterwards, the minimum required position accuracy will be determined, delivering insights about the adequate positioning methods and radiolocation technologies. In particular the additional resources to be committed to achieve sufficient interference map accuracy will be derived with respect to the primary system deployment scenarios (i.e. radio relying on LTE only, or LTE+UWB, of UWB only, radiolocation involving non-cooperative with respect to fixed anchors only or also cooperative links, etc.).

5 CALIBRATION FRAMEWORK FOR PHYSICAL LAYER ABSTRACTION OF (TURBO) CODEWORD IC RECEIVERS

5.1 Introduction

Within the evolution of wireless systems, the cross layer optimization between PHYlayerand MAC has drawn a lot of attention, due to the improved data rate and QoS it offers. InMIMOtransmissions, the PHY-MAC cross layer design is based on mechanisms such as Fast Link Adaptation (FLA), which exploits the instantaneous feedback from the receiver to inform the transmitter about the radio link quality (see, e.g., [JKW10]). The key idea of the FLA mechanisms are to predict the Packet Error Rate (PER) for different Modulation and Coding Schemes (MCSs) in order to select the MCSs together with the MIMO precoding that maximize the throughput under a certain QoS constraint (10% PER in LTE). Therefore, accurate and fast prediction of the link-level performance at the receiver side is of paramount importance for advanced mobile communications. Due to the constraints of limited feedback and finite size precoding codebooks, the residual interference at the receiver output remains a major impediment to reach the high MIMO spectral efficiencies promised by information theory. That is why advanced receivers regain a lot of attention in 3GPP [3GPP12]. Among them, the turbo Linear CodeWord Interference Cancellation (turbo L-CWIC) receivers in 3GPP, offer a particularly interesting trade-off between complexity and performance. As a result, PHY abstractions, that are able to capture their behavior in order to derive precisely the limited feedback metrics is of great interest in practice. The conventional PHY abstractions rely on the assumption that an analytical SINR formula exists. Nonetheless, in the case of reduced complexity ML receiver, reference [LKP13] proposes to use approximate SINRs that results from the calibrated combination of the Linear Minimum Mean Square Error (LMMSE) SINR and the Genie Aided SNR (the Genie Aided SNR models a receiver that can remove perfectly the interference).

In this work, we address the design of PHY abstractions for the class of turbo L-CWIC receivers. We build our work on previous research studies in this field, e.g., [CVS08,LKP13] The proposed PHY abstraction is inspired from the EXtrinsic Information Transfer (EXIT) chart framework [NVB13] which underlines the MIESM compression technique [BAS05]. The key idea is to estimate at a given iteration the ESM at the output of the LMMSE filters, then to calculate the Interference Estimation Reliability (IER) variance for the next iteration. The IER variance along with the CSIR, are able to reproduce the ESM for the next iteration and so on. In [NVB13], a one-dimensional (1D) calibration has been proposed to minimize the prediction error caused by invalid assumptions inescapable for the sake of SINR derivation. These assumptions yields too optimistic PER predictions. Herein, we revisit the calibration method by proposing a more rigorous framework to minimize the predicted throughput error that dramatically influences the FLA mechanisms. We also suggest a novel multi-dimensional calibration approach that corrects the ESM by both increasing the IER variance and applying two correction factors to the MIESM compression.

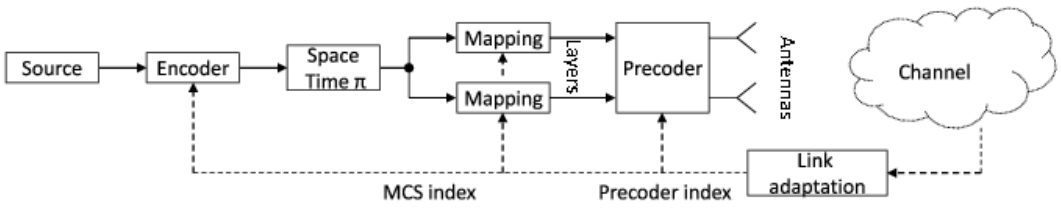

Figure 15: STBICM transmission scheme within a FLA framework.

5.2 System model

We consider a single-user coded MIMO transmission over a flat block Rayleigh fading channel. It is a building block for any extension to multi-user coded MIMO transmission [VBL10]. The transmitter and receiver are equipped with n_t transmit and n_r receive antennas, respectively. The number of channel blocks is denoted by n_b and the total number of channel uses L. The channel is assumed to be perfectly known

at the receiver. The MIMO coding scheme is a Space-Time Bit Interleaved Coded Modulation (STBICM). The transmission scheme is exhibited in Figure 15 within a FLA framework. The binary information are firstly encoded using a linear channel encoder. Then, the encoder output is space-time interleaved to yield the interleaved coded bits per antenna which are finally modulated independently with Gray labeling. The modulated symbol vectors are then sent over the space time dimensions or channel uses. Let $\mathrm{H_b} \in \mathbb{C}^{\mathrm{n_r} \times \mathrm{n_t}}$ denotes the channel for the b-th fading block. The received vector $\mathrm{y_{b,l}} \in \mathbb{C}^{\mathrm{n_r}}$ at the destination during the b-th fading block and channel use $\mathrm{l} = 1, \cdots, \mathrm{L}/\mathrm{n_b}$ is expressed as

$$\mathbf{y_{b,l}} = \mathbf{H_b s_{b,l}} + \mathbf{w_{b,l}}. \tag{5.42}$$

In (4.40), the modulated symbol vectors $\mathrm{s_{b,l}} = [\mathrm{s_{b,1,l}}, \cdots, \mathrm{s_{b,n_t,l}}]^{\mathrm{T}}$ are i.i.d. random vectors with $\mathbb{E}[\mathrm{s_{b,l}}] = 0_{\mathrm{n_t}}$ and $\mathbb{E}[\mathrm{s_{b,l}} \mathrm{s_{b,l}^{\dagger}}] = \mathrm{I_{n_t}}$, and the vectors $\mathrm{w_{b,l}} \in \mathbb{C}^{\mathrm{n_r}}$ are i.i.d. random vectors, circularly-symmetric Gaussian, with zero-mean and covariance matrix $\mathrm{R} = \sigma^2 \mathrm{I_{n_r}}$. The channel coefficients are normalized such that $\rho = 1/\sigma^2$ is the average SNR per receive antenna. We denote $\underline{\mathrm{h}} = \mathrm{vec(H)}$ and $\underline{\mathrm{c}} = [\mathrm{vec(H)}^{\mathrm{T}}, \rho]^{\mathrm{T}}$ the channel coefficients and the CSIR, where $\mathrm{H} = [\mathrm{H_1} \ \cdots \ \mathrm{H_{n_b}}]$ where $\mathrm{vec(H)} = \left[\mathrm{h_1^T}, \ldots, \mathrm{h_n^T}\right]^{\mathrm{T}}$, $\mathrm{h_i}$ being the i-th column of H

Note that STBICM with linear precoding is straightforwardly encompassed by including the precoder into the channel H.

5.3 LAPPR-based turbo L-CWIC

5.3.1 Turbo L-CWIC architecture

We consider in the following the LMMSE-IC with parallel scheduling since the coding is performed across antennas in STBICM. The first step is to subtract the interference estimated from the previous iteration. The resulting signal is then filtered and demapped to its original binary form. The resulting bits are de-interleaved according to the space-time interleaving rule applied at the transmitter. The channel code is a turbo code similar to what is implemented in LTE. Once the activation of the turbo-decoder provides Log Likelihood Ratios (LLRs) on the coded bits, the interference can be estimated and subtracted to all blocks and antennas. The interference soft estimationis based on the Log A posteriori Probability Ratios (LAPPRs) Λ_{ap}, which is the total output of the channel decoder (including channel observations). In the following, we adopt the latter approach, coined LAPPR-based turbo L-CWIC, since it provides (in general) better performance [BRI99] and is the most difficult to predict [WBS02].

5.3.2 PHY abstraction

The PHY abstraction framework relies on symbol-wise semi-analytical prediction performance. The proposed methods consider the user demapping and decoding as a joint process and tracks the evolution of the Average Mutual Information (AMI) defined at symbol level and circulating between the LMMSE-IC based interface and the bank of joint demappers and channel decoders. Figure 16 describes the two parts of the abstraction scheme for turbocoded transmission. The first part ends up with a $\mathrm{n_b}.\mathrm{n_t}$ parallel channel at a given iteration. Each sub-channel is modelled as a discrete-input Additive White Gaussian Noise (AWGN) channel, i.e. $\tilde{\mathrm{s}}_{\mathrm{b,t,l}} = \mathrm{s_{b,t,l}} + \varepsilon_{\mathrm{b,t,l}}$ with $\varepsilon_{\mathrm{b,t,l}} \sim \mathcal{N}_{\mathbb{C}}(0, \frac{1}{\gamma_{\mathrm{b,t}}})$ where $\gamma_{\mathrm{b,t}}$ is the SINR value at $\mathrm{b-th}$ block and $\mathrm{t-th}$ antenna. The latter parallel channel AMI can be obtained by averaging the AMI with respect to $\gamma_{\mathrm{b,t}}$ of each sub-channel. $\mathrm{x} \sim \mathcal{CN}(\mu, \sigma^2)$ means that x is a circularly-symmetric complex Gaussian RV with mean μ and variance σ^2. Finally, the so-called effective SINR γ_{eff} (or MIESM) is the SNR that yields the same AWGN channel AMI as the one of the original parallel channel. The second part relies on prediction transfer functions describing the channel decoder. For a turbo-code, these functions are the $\mathrm{LUT_{PER}}$ yielding the PER, the $\mathrm{LUT_{\nu}}$ yielding the IER variance ν, and the $\mathrm{LUT_{MI}}$ yielding the mutual information $\mathrm{I_{in}}$ on the systematic bits originating from the turbo-decoder last iteration. The 3 LUTs represents sampled functions simulated off-line on an AWGN channel that are bi-dimensional with respect to $\mathrm{I_{in}}$ and γ_{eff} (see [VBL10] for more details). For the next iteration, the effective SINR is updated with the new IER variance read out from the $\mathrm{LUT_{\nu}}$ and the mutual information from the $\mathrm{LUT_{MI}}$ and the process is repeated. Since we aim at

predicting LAPPR-based turbo L-CWIC most of the PHY abstraction underlying assumptions are violated [VBL10]. As a result, we have to resort to some calibration methods to improve its accuracy in average.

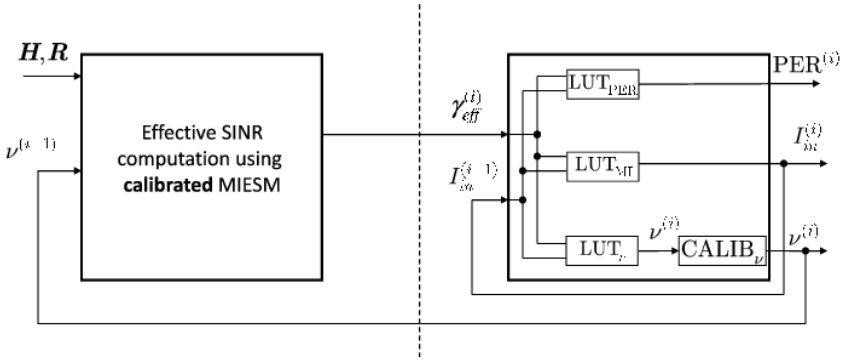

Figure 16:PHY abstraction for turbo L-CWIC at iteration*i*.

5.4 PHY abstraction calibration

A 1D calibration over the IER factor read out from the LUT_{ν} was proposed in [NVB13]. The IER at iteration $\mathrm{i} = 1, \cdots, \mathrm{it}$ is obtained as

$$\nu^{(i)} = \mathrm{LUT}_{\nu}\left(\gamma_{eff}^{(i)}\left(\underline{\mathbf{c}}, \nu^{(i-1)}\right), I_{in}^{(i-1)}\right), \tag{5.43}$$

and the MI as

$$I_{in}^{(i)} = \mathrm{LUT}_{\mathrm{MI}}\left(\gamma_{eff}^{(i)}\left(\underline{\mathbf{c}}, \nu^{(i-1)}\right), I_{in}^{(i-1)}\right), \tag{5.44}$$

where $\mathrm{I}_{\mathrm{in}}^{(0)}$ and $\nu^{(0)}$ takes the value of 0 and 1, respectively, for the first iteration. The initially proposed 1D calibration consists in replacing the IER variance $\nu^{(\mathrm{i})}$ by $\nu^{(\mathrm{i})} \leftarrow \min(1, \alpha_0 \nu^{(\mathrm{i})})$ where $\alpha_0 \geq 1$ is sought in order to minimize the error between the predicted and simulated average PER in a given region [VBL10]. Here, we propose an improved calibration framework which minimizes the error between the predicted and simulated instantaneous PER, i.e., the PER with respect to a given CSIR outcome, at the targeted iteration number it. It is clearly the most rigorous approach to calibrate our PHY abstraction for FLA applications. Furthermore, we suggest a general calibration framework which also calibrates the MIESM compression at each iteration $\mathrm{i} = 1, \cdots, \mathrm{it}$. It can be expressed as follows, omitting the CSIR and IER dependency,

$$\gamma_{eff}^{(i)}(\alpha^{(i)}) = \alpha_2^{(i)} I^{-1}\left(\frac{1}{n_t . n_b} \sum_{t=1}^{n_t} \sum_{b=1}^{n_b} I\left(\frac{\gamma_{b,t}^{(i)}(\alpha_0^{(i-1)})}{\alpha_1^{(i)}}\right)\right) \tag{5.45}$$

where $\alpha^{(\mathrm{i})} = [\alpha_0^{(\mathrm{i}-1)}, \alpha_1^{(\mathrm{i})}, \alpha_2^{(\mathrm{i})}]^{\mathrm{T}}$, $\mathrm{I}(.)$ is the mutual information for a given discrete input and $\gamma_{\mathrm{b,t}}^{(\mathrm{i})}(\alpha_0^{(\mathrm{i}-1)})$ is the SINR at iteration i related to block b and antenna t whose analytical formula with respect to the CSIR and $\nu^{(\mathrm{i}-1)} \leftarrow \min(1, \alpha_0^{(\mathrm{i}-1)} \nu^{(\mathrm{i}-1)})$ is detailed in[NVB13]. Note that the 1D calibration framework is included when the following constraints $\alpha_1^{(\mathrm{i})} = \alpha_2^{(\mathrm{i})} = 1$, $\alpha_0^{(\mathrm{i})} = \alpha_0$ for all $\mathrm{i} = 1, \cdots, \mathrm{it}$ and $\alpha_0^{(0)} = 1$ are applied. Next Section describes the Monte Carlo framework to obtain the calibration factors.

5.4.1 Calibration methods

PHY abstractions are mainly used in practice for FLA. Indeed, as stated in the introduction, FLA is an essential feature of advanced mobile systems. As a result, our calibration procedure aims at minimizing the Mean Squared Error (MSE) between the simulated and predicted throughput at the targeted iteration number it. More precisely, the throughput prediction error in FLA scheme is

$$\varepsilon_1 = \int \left| R_{\mathrm{p}}^{(it)}(\underline{\mathbf{c}}) - R_{\mathrm{s}}^{(it)}(\underline{\mathbf{c}}) \right|^2 p(\underline{\mathbf{c}}) d\underline{\mathbf{c}} \tag{5.46}$$

where $R_s^{(it)}(\underline{c})$ and $R_p^{(it)}(\underline{c})$ are the predicted and simulated throughput, respectively, at iteration it and with respect to the CSIR $\underline{c}$, $p(\underline{c})$ is the PDF of the CSIR. We have $p(\underline{c}) = p(\underline{h})p(\rho)$ where $p(\underline{h})$ and $p(\rho)$ are the pdf of the channel coefficients and the average SNR. It yields for a given MCS of rate R_m

$$\varepsilon_2 = \varepsilon_1 / R_m^2 = \int \left| \mathrm{PEP}_m^{(it)}(\underline{\mathbf{c}}, \underline{\boldsymbol{\alpha}}) - \mathrm{PER}_m^{(it)}(\underline{\mathbf{c}}) \right|^2 p(\underline{\mathbf{c}}) d\underline{\mathrm{c}} \tag{5.47}$$

where PEP $_m^{(it)}(\underline{c}, \underline{\alpha})$ and PER $_m^{(it)}(\underline{c})$ are the predicted and simulated PER at iteration it for the given CSIR $\underline{c}$ and MCS $m$and $\underline{\alpha} = [\alpha^{(1)^T}, \cdots, \alpha^{(it)^T}]^T$. Finding the calibration factors that minimize the predicted throughput errors leads to the following optimization problem

$$\underline{\boldsymbol{\alpha}} = \min_{\underline{\boldsymbol{\alpha}}} \varepsilon_2(\underline{\boldsymbol{\alpha}}) = \mathbb{E}_{\underline{c}}\left[\left| \Delta\mathrm{PEP}_m^{(it)}(\underline{\mathbf{c}}, \underline{\boldsymbol{\alpha}}) \right|^2 \right] \tag{5.48}$$

where $\Delta\mathrm{PEP}_m^{(it)}(\underline{c}, \underline{\alpha}) = \mathrm{PEP}_m^{(it)}(\underline{c}, \underline{\alpha}) - \mathrm{PER}_m^{(it)}(\underline{c})$. In the following, we omit the dependency of the PER, PEP and ΔPEP with respect to the iteration number it and MCS number m for the sake of notation simplicity. Calibration optimization procedure

Our Goal is to minimize the discrepancy between the simulated and predicted data rate. It comes down to minimizing the average MSE between the simulated and predicted instantaneous PER as explained in the previous Section. It is well known that the maximization of the throughput in FLA, i.e., $\max_m R_m(1 - \mathrm{PER}_m)$, have the MCS used in the PER region of $[0.1,1]$. In LTE, the feedback metrics are chosen for a target PER of 10%. It is also the region where PER prediction errors have the worst effect on the MSE given in (6). That is why we focus on that region in the following. Since the prediction method should work irrespective of the channel outcome, we perform our calibration on the worst channel and noise variance pdfs, the worst in terms of spread of the CSIR outcomes following the maximum entropy principle. Therefore, the random vector $\underline{h}$ pdf is chosen to follow a multidimensional circularly complex Gaussian distribution with covariance proportional to the identity matrix and the average SNR pdf is uniformly distributed between $[\rho_{\min}, \rho_{\max}]$. The SNR limits are chosen such that the probabilities that $\mathrm{PER}(\underline{h}, \rho_{\min}) = 1$ and that $\mathrm{PER}(\underline{h}, \rho_{\max}) < 10\%$ is close to 1. In practice, we choose a sufficiently large SNR range, e.g., -30dB and $+30$dB. We define the subset Ω as the event that the simulated PER is between $[0.1,1]$, which is the region of interest. Let us define the random variable $X(\underline{c}) = [\underline{c} \in \Omega]$, where the Iverson bracket $[P]$ yields 1 if the event P is true and 0 otherwise. Finally, our calibration method can be expressed as

$$\underline{\boldsymbol{\alpha}} = \min_{\underline{\boldsymbol{\alpha}}} \mathbb{E}_{\underline{c}}\left[X(\underline{\mathbf{c}}). \left| \Delta\mathrm{PEP}(\underline{\boldsymbol{\alpha}}, \underline{\mathbf{c}}) \right|^2 \right] = \min_{\underline{\boldsymbol{\alpha}}} \varepsilon(\underline{\boldsymbol{\alpha}}). \tag{5.49}$$

The cost function in this equation can be expanded into

$$\varepsilon(\underline{\boldsymbol{\alpha}}) = \frac{1}{\Delta\rho} \int p(\underline{\mathbf{h}}) d\underline{\mathrm{h}} \int_{\rho_{\min}}^{\rho_{\max}} d\rho X(\underline{\mathbf{c}}) \left| \Delta\mathrm{PEP}(\underline{\boldsymbol{\alpha}}, \underline{\mathbf{c}}) \right|^2 \tag{5.50}$$

where $\Delta\rho = \rho_{\min} - \rho_{\max}$. Using Monte Carlo and trapezoidal rule (with non uniform step) integration methods, it can be evaluated as

$$\varepsilon(\underline{\boldsymbol{\alpha}}, N) = \frac{1}{N\Delta\rho} \sum_{n=1}^{N} \sum_{m=0}^{M_n - 1} \frac{\eta_{n,m}}{2} \left(\delta_{n,m} + \delta_{n,m+1} \right) \tag{5.51}$$

where

$$\begin{cases} \delta_{n,m} &= |\Delta\mathrm{PEP}(\underline{\boldsymbol{\alpha}}, \underline{\mathbf{h}}_{\boldsymbol{n}}, \rho_{n,m})|^2 \\ \rho_{n,m+1} &= \rho_{n,m} 10^{\frac{\Delta_{n,m}}{10}} \\ \eta_{n,m} &= \rho_{n,m} (10^{\frac{\Delta_{n,m}}{10}} - 1) \end{cases}, \tag{5.52}$$

and where h_n is drawn following the distribution $p(\underline{h})$, $M_n + 1$ is the number of SNR points starting at SNR $\rho_{n,0}$ and increasing by varying steps $\{\Delta_{n,m}\}$ in dB to reach ρ_{n,M_n} conditional on the given channel outcome $\underline{h}_n$, N is the total number of channel outcomes considered. The parameters $M_n + 1$, $\{\Delta_{n,m}\}$, $\rho_{n,0}$,N should be wisely selected in order to accurately match the MSE ε. The starting SNR point $\rho_{n,0}$ is selected such that the PEP($\underline{h}_n, \rho_{n,0}$) without calibration is equal to 1 while the PEP($\underline{h}_n, \rho_{n,1}$) is between $[0.95,1[$. Indeed, we know from [NVB13] that PER≥PEP without calibration (the prediction is too optimistic), and thus ΔPEP$= 0$ when PEP$= 1$. The SNR steps $\{\Delta_{n,m}\}$ should be sufficiently small to capture the smoothness of the simulated PER curve. Finally, $M_n + 1$ (or the final SNR ρ_{n,M_n}) is chosen to reach a simulated PER below 0.1. The number of channel N should satisfy the convergence criterion defined as

$$\varepsilon(\underline{\boldsymbol{\alpha}}, N) = \lim_{n\to\infty} \varepsilon(\underline{\boldsymbol{\alpha}}, n). \tag{5.53}$$

5.5 Simulation results

We consider an STBICM transmitted over 4×4 quasi-static Rayleigh n_b block fading, the number of channel blocks is either $n_b = 1$ or $n_b = 8$. The STBICM is built from a turbo code based on two 8-state recursive systematic convolutional encoders with generator matrix $G = [1,1011/1101]_2$ and Gray labeling with QAM modulation. The evaluation is performed for MCS 6 whose rate is $R = n_t q_1 r_1 = 8$ bits per channel use (bpcu) where $r_1 = 1/2$ is the punctured turbo code rate and $q_1 = 4$ is related to a 16QAM modulation and for MCS 12 whose rate is $R = n_t q_2 r_2 = 20$ bpcu where $r_2 = 5/6$ is the punctured turbo code rate and $q_2 = 6$ is related to a 64QAM modulation. These MCSs are chosen since they are particularly difficult to predict due to their very high spectral efficiencies. Indeed, MCS 12 is all the more difficult since it combines both a high code rate and high modulation order, thus the calibration procedure is crucial. The total number of channel uses is fixed to $L = 2040$. The number of iterations is chosen in order to have the performance converged, i.e., $it = 8$, only one inner turbocode iteration is performed. In the following, we refer to MSE as the relative MSE $\Delta\rho\varepsilon(\underline{\alpha})$ where $\Delta\rho \approx 10^3$.

Table 2: 8-block fading channel - 1D/3D calibration factors

MSE	w/ocalib.	1D calib.	3D calib.	8D calib.
MCS 6	0.35	0.01	0.0078	0.0058
MCS 12	7.67	0.56	0.406	0.403

Table 3: 1-block fading channel - MSE

MSE	w/ocalib.	1D calib.	3D calib.	8D calib.
MCS 6	0.51	0.037	0.0209	0.017
MCS 12	9.58	0.54	0.397	0.38

In order to carry out the calibration and to estimate the MSE given in (5.54), we start by generating the trace files (TF) for MCS 6 and MCS 12. Each TF contains a set $\mathcal{H}$ of channel realizations with their simulated PER in the interval $[0.1,1]$. We apply the PHY abstraction scheme on the saved channel outcomes and we compute the MSE between simulated and predicted instantaneous PER. Fig. 4 illustrates a batch of curves for MCS 6 and 12. The simulated PER are shown for more than 60 channel outcomes for each MCS. We witness that fixing $\Delta_{n,m} = 0.1\text{dB}\forall n, m$ for all channel outcomes was sufficient with acceptable computational time complexity. It can be observed that the MCS 12 performance is more dispersed over the SNR interval than MCS6. This dispersion is due both to the high coding rate and the 64QAM modulation.

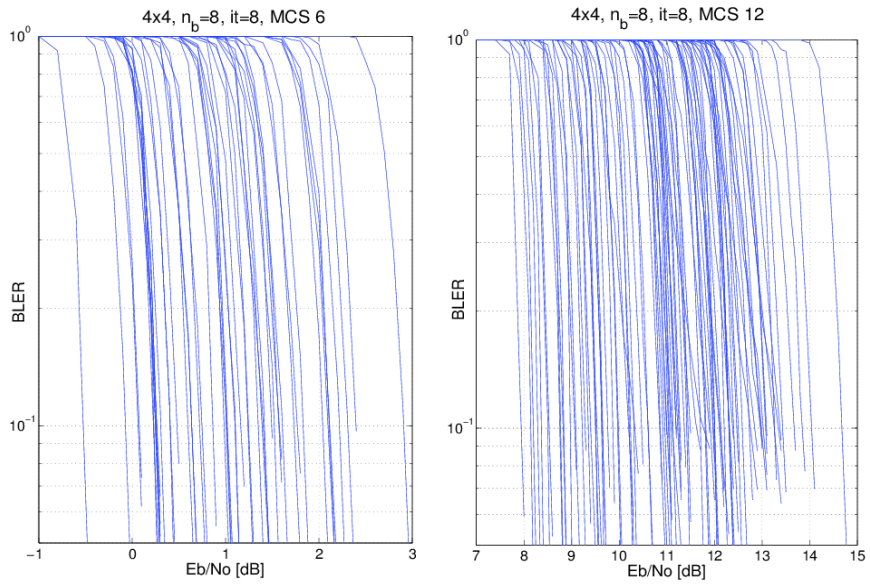

Figure 17: Batch of curves stocked in the Trace files in order to perform the calibration for MCS 6 and MCS12.

Regarding the optimization problem introduced in (4.47) for calibration, it can be resolved using numerical algorithms such as the Polak-Ribiere conjugate gradient. The latter is implemented in C by the GNU Scientific (GSL) library [GOU09] which was used in the paper. In order to show that the number of channel outcomes N in the TFs is enough to satisfy the MSE convergence (4.51), we plot inFigure 18 the optimized MSE, i.e., with optimal calibration factors for each value of N, with respect to N. For MCS 6, the minimal MSE largely fluctuates when N is small, i.e. $N < 20$. The convergence is achieved with the increase of N, i.e. $N > 20$. For MCS 12, a higher number of random channel realizations is required and the convergence region starts for $N > 60$.

After having checked the convergence, the calibration efficiency is evaluated based on the MSE, representative of the throughput prediction error.Table 2compares the non calibrated MSE to the 1D, 3D and 8D calibrated ones in 8-block fading channel.We mean by 3D calibration that α is constant over all iterations, and by 8D calibration that α is optimized for the first 3 iterations, i.e., the optimization is carried over $\alpha^{(1)}$, $\alpha^{(2)}$ and $\alpha^{(3)}$ with the following constraints $\alpha^{(i)} = \alpha^{(3)}\ \forall i > 3$ and $\alpha_0^{(0)} = 1$. It can be seen that the calibration introduces a significant MSE gain, and that the 3D calibration results in additional gain compared to the 1D approach. For MCS 12, the MSE decreases from 7.67 to 0.56 using the 1D calibration and then to 0.4 using the 3D calibration.The 8D calibration results in an additional gain for MCS 6, however, for MCS 12 this gain is not as noticeable. In 1-block fading channel, similar observations are made as shown in Table 3, i.e. , for MCS 6 the MSE decreases from 0.51 to 0.037 using the 1D calibration, then to 0.0209 using the 3D calibration, and to 0.017 using the 8D calibration.Comparing the 1D calibration factors with respect to the 1-block and 8-block fading cases, we can conclude that for MCS 6 and MCS 12 the calibration factors are close, and that the optimal calibration factors for 8-block fading channel yield an MSE near to optimal when applied to the 1-block fading channel as shown inTable 4.Thus, rough calibration factors could be used (e.g., by taking the highest calibration factor value) in the 1D case which confirms our previous conclusions of low dependency of the proposed PHY abstraction with the frequency selectivity of the channel.

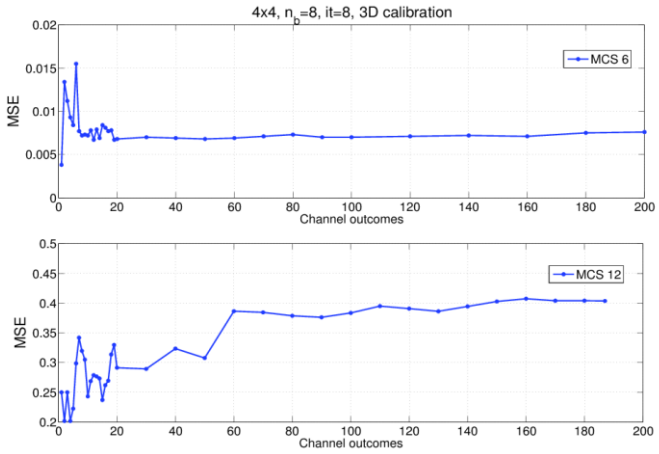

Figure 18:The convergence of the 3D MSE calibration solution for MCS 6 and MCS 12.

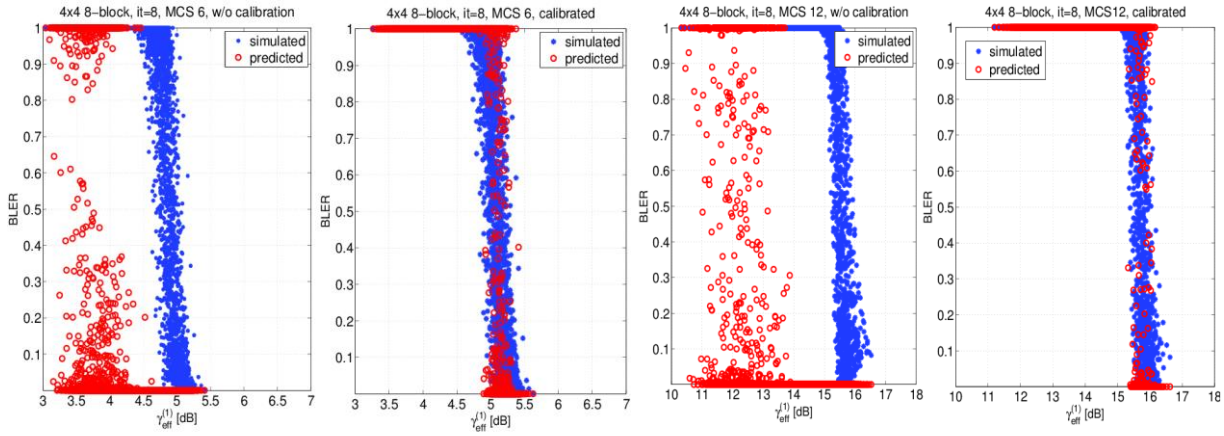

Figure 19: Comparison of the predicted and simulated PER for MCS 6 and MCS 12.

Finally, we show the calibration effect with respect to the effective SINR at first iteration denoted $\gamma_{\text{eff}}^{(1)}$ for simplicity. Figure 18 and Figure 19 illustrate the impact of the 3D calibration on the PEP for 8-block fading channel. In the non-calibrated scheme, for MCS 6 and $\gamma_{\text{eff}}^{(1)}$ between $3-4.5$ dB and for MCS 12 and $\gamma_{\text{eff}}^{(1)}$ between $10-15$ dB, many predicted PER are in the interval $]0,0.1]$ whereas the simulated PER are at 1. After 3D calibration, all those aforementioned points are corrected and brought back to their simulated value. This explains the significant decrease in the MSE in Table 4.

Table 4: 1-block fading MSE w.r.t. the calibration coefficients optimized for 8-block fading channel

MSE	1D calib.	3D calib.	8D calib.
MCS 6	0.046	0.023	0.020
MCS 12	0.58	0.56	0.56

The future work is to integrate the HARQ-Type II Chase Combining scheme in the turbo-CWIC, and to evaluate the throughput in FLA context under low, medium and high correlated channel.

6 CONCLUSIONS

This deliverable presents novel approaches for interference management in realistic networks. The different stages leading to a comprehensive interference management solution are studied, from the design of a model for the wireless network and the interference created, to the abstraction of the performance. It is shown that by properly taking into account the practical constraints, it is possible to design new robust methods with a strong potential for reducing significantly the interference floor in future networks. The methods presented are highly innovative and are based on new ideas. Preliminary simulation results are presented to show the potential of the approach and help in understanding its main principle. However, how to make these methods more efficient in practice and more advanced performance evaluation will be carried out in the future in order to evaluate more precisely the possible gains.

REFERENCES

[3GPP11] FDD Base Station (BS) classification, 3GPP TR 25.951 v.10.0.0 Std., May 2011.

[3GPP12] 3GPP "Network-assisted interference cancellation and suppression for LTE," Technical Report 36.866 V1.1.0, Release 12.

[AS64] M.Abramovitz, I.A.Stegun "Handbook of Mathematical Functions with Formulas, Graphs and Mathematical Tables", National Bureau of Standards Applied Mathematics Series 55, June 1964.

[BAS05] K. Brueninghaus, D. Astely, T. Sälzer, S. Visuri, A. Alexiou, S. Karger, and G.-A. Seraji, "Link performance models for system level simulations of broadband radio access systems," in proc. IEEE International Symposium on Personal, Indoor and Mobile Radio Communications (PIMRC),2005.

[BB09] F. Baccelli and B. Blaszczyszyn, "Stochastic geometry and wireless networks: volume I - Theory", NoW Publishers, Foundations and Trends in Networking,2009.

[BHA11] A. Babaei, M. Haenggi, P. Agrawal, and B. Jabbari, "Interference statistics of a poisson field of interferers with random puncturing,"in Military Communications Conference (MILCOM), 2011.

[BPG10] L. Brunel, M. Plainchault, M. Gresset, N. Dammann, C. Mensing, and R. Raulefs, "Inter-Cell Interference Coordination and Synchronization based on Location Information", in proc. Positioning Navigation and Communication workshop (WPNC'10), 2010.

[BRI99] S. ten Brink, "Convergence of iterative decoding," IEE Electron. Lett., vol. 35, pp. 806–808, 1999.

[CL09] Y. Corre and Y. Lostanlen, "Three-dimensional urban EM wave propagation model for radio network planning and optimization over large areas", IEEE Transactions on Vehicular Technology, vol. 58, no. 7, pp. 3112-3123, Sept. 2009.

[CVS08] A. M. Cipriano, R.Visoz, and T.Salzer, "Calibration issues of phy layer abstractions for wireless broadband systems," Proc. IEEE VTCF, Calgary, Canada, Sept. 2008.

[D3.1] SHARING deliverable D3.1, "New opportunities, challenges and innovative concepts candidates for Multi-point transmission and reception".

[D3.2] SHARING deliverable D3.2, "Multi-point cooperation schemes at the transmitter: innovative concepts and performance evaluation".

[D4.2] SHARING deliverable D4.2, "Intra-system offloading: innovative concepts and performance evaluation".

[DA13] H. S. Dhillon and J. G. Andrews, "Downlink rate distribution in heterogeneous cellular networks under generalized cell selection," IEEE Wireless CommunicationsLetters, 2013.

[DER14] Demange, T. Ekim, B. Ries, and C. Tanasescu, "On some applications of the selective graph coloring problem", European Journal of Operational Research, 2014.

[DFM09] L. Decreusefond, E. Ferraz, and P. Martins, "Upper Bound of Loss probability for the dimensioning of OFDMA systems with multi class randomly located users",in proc. International Symposium on Modeling and Optimization in Mobile, Ad Hoc and Wireless Networks (Wiopt), workshop, 2009.

[DGB12] H.S. Dhillon, R. K. Ganti, F. Baccelli, and J. G. Andrews, "Modeling and analysis of k-tier downlink heterogeneous cellular networks",IEEE journal on Selected Area in Communications, vol. 30, no. 3, pp. 550-560, 2012.

[DMM14] S. Deb, P. Monogioudis, J. Miernik, and J.P. Seymour, "Algorithms for Enhanced Inter-Cell Interference Coordination (eICIC) in LTE HetNets", in IEEE/ACM transactions on networking, vol. 22, NO. 1, pp. 137-150, 2014.

[E-UTRA10] Evolved Universal Terrestrial Radio Access (E-UTRA); Further advancements for E-UTRA physical layer aspects (Release 9), 3 GPP TR 36.814, V9.0.0 Std., march 2010.

[GHH10] D. Gesbert, S. Hanly, H. Huang, S. ShitzShamai, O. Simeone, and Wei Yu, "Multi-Cell MIMO Cooperative Networks: A New Look at Interference",IEEE journal on Selected Area in Communications, vol. 28, no. 9, pp. 1380-1408, 2010.

[GBG11] J. Guillet, L. Brunel, and N. Gresset, "Downlink femto-macro ICIC with blind long-term power setting," in proc. Personal Indoor and Mobile Radio Communications (PIMRC'11), 2011.

[GH14] Z. Gong and M. Haenggi, "Interference and outage in mobile random networks: Expectation, distribution, and correlation," IEEE transaction on mobile computing, vol. 13, no. 2, February 2014.

[GOU09] B. Gough, "Network Theory", GNU scientific library reference manual, 2009.

[GWC13] W. Guo, S. Wang, X. Chu, J. Zhang, J. Chen and H. Song, "Automated Small-Cell Deployement for Heterogeneous Cellular Networks," IEEE communication magazine, May, 2013.

[HKB12] R. W. Heath Jr, M. Kountouris, and T. Bai, "Modeling heterogeneous network interference using Poisson point processes," arxiv: 1207.2041, july, 2012. [Online] available: arxiv.org/abs/1207.2041

[JAF14] S. Jafar, "Topological interference management through index coding," IEEE Trans. Information Theory, vol. 60, no. 1, pp. 529–568, Jan. 2014.

[JKW10] T.L. Jensen, S.Kant, J.Wehinger, and B.H. Fleury, "Fast link adaptation for MIMOOFDM", IEEE Trans. Veh. Technol., vol.VT-59, pp. 3766–3778, Oct. 2010.

[JSX12] H. S. Jo, Y. J. Sang, P. Xia, and J. G. Andrews, "Heterogeneous Cellular Networks with Flexible Cell Association: A Comprehensive Downlink SINR Analysis," IEEE transaction on wireless communications, vol. 11, no. 10, 2012.

[KBK13] H.-P. Keeler, B. Blaszczyszyn, and M. Karray, "Sinr-based k-coverage probability in cellular networks with arbitrary shadowing", in proc. IEEE international Symposium on Information Theory (ISIT), 2013.

[KG14] P. de Kerret and D. Gesbert, "Interference alignment with incomplete CSIT sharing" , IEEE Trans. Wireless Communications, vol. 13, no. 5, pp.2563-2573, May 2014.

[KMD13] F. Z. Kaddour, P. Martins, L. Decreusefond, L. Mroueh, and E. Vivier, "Outage probability upper's bound in uplink long term evolution networks with multi QoS users classes" , Proc. IEEE Global Communications Conference (GLOBECOM), 2013.

[KVP12] F. Z. Kaddour, E. Vivier, M. Pischella, and P. Martins, "A new method for inter-cell interference estimation in uplink SC-FDMA networks", in IEEE Vehicular technology Conference (VTC), 2012.

[LBL13] C. H. de Lima, M. Bennis, and M. Latva-aho, "Statistical analysis of self-organizing networks with biased cell association and interference avoidance," IEEE Transaction on Vehicular Technology, vol. 62, no. 5, June 2013.

[LBC10] C. de Lima, M. Bennis, K. Chaboosi, and M. Latva-aho, "On interference analysis of self-organized femtocells in indoor deployment,"", Proc. IEEE Global Communications Conference (GLOBECOM), 2010.

[LET14] E. G. Larsson, O. Edfors, F. Tufvesson, and T. L. Marzetta, "Massive MIMO for next generation wireless systems," in IEEE communication Magazine, February 2014.

[LKP13] H.Lee, T.Kim, W.Park, and J.Lim, "Link performance abstraction for interference-aware communications (iac)," arXiv preprint arXiv:1310.0872, 2013.

[NA13] N. Naderializadeh and A. S. Avestimehr, "Interference networks with no CSIT: Impact of topology," submitted to IEEE Trans. Information Theory, arXiv:1302.0296, Feb. 2013.

[NVB12] B. Ning, R. Visoz, A.O. Berthet, "Extrinsic versus a posteriori probability based iterative LMMSE-IC algorithms for coded MIMO communications: Performance and analysis", in Proc. IEEE International Symposium on Wireless Communication Systems (ISWCS12), 2012.

[NVB13] B. Ning, R. Visoz, and A. O. Berthet, "Physical layer abstraction for turbo coded MIMO systems with LMMSE-IC based turbo equalization", Proc. IEEE Global Communications Conference (GLOBECOM), 2013.

[OIS12] H. Osada, M. Inamori, and Y. Sanada, "Non-orthogonal Access Scheme over Multiple Channels with Iterative Interference Cancellation and Fractional Sampling in OFDM Receiver",Proc.Vehicular Technology Conference (VTC Spring), 2012.

[PT04] K. Pomorski and K. F. Teoretycznej, "Gauss-hermit approximation formula," April 2004. [Online]. Available: arxiv.org/pdf/physics/0404018.pdf

[SKM87] D. Stoyan, W. Kendall, J. Mecke, and L. Ruschendorf, "Stochastic geometry and

itsapplications", Wiley New York, 1987, vol. 2.

[TSS12] Thien-Toan Tran, Yoan Shin, Oh-Soon Shin, "Overview of Enabling Technologies for 3GPP LTE-Advanced, " EURASIP Journal on Wireless Communications and Networking, 2012

[VBL10] R.Visoz, A.O. Berthet, and M. Lalam, "Semi-analytical performance prediction methods for iterative MMSE-IC multiuser MIMO joint decoding," IEEE Trans. Commun., vol.58, no.9, pp. 2576–2589, Sept. 2010.

[WBS02] M. Witzke, S. Bäro, F. Schreckenbach, J. Hagenauer, "Iterative Detection of MIMO Signals with Linear Detectors," Proc. Asilomar Conference on Signals, Systems and Computers,2002.

[WES01] D. B. West et al., "Introduction to graph theory", Prentice hall Englewood Cliffs, vol. 2, 2001.

[WG13] S. Wang and W. Guo,"Mobile crowd-sensing wireless activity with measured interference power," IEEE wireless communications letters, vol. 2, no. 15, October 2013.

[WG14] S. Wang and W. Guo, "Downlink interference estimation without feedback for heterogeneous network interference avoidance," in Proc. International Conference on Telecommunications (ICT), Lisbon, Portugal, May 2014.

[YG14] X. Yi and D. Gesbert, "Topological interference management with transmitter cooperation," submitted to IEEE Trans. Information Theory, Jul. 2014, under revision.

[ZH14] X. Zhang and M. Haenggi, "A stochastic geometry analysis of inter-cell interference coordination and intra-cell diversity", arxiv: 1403.0012 v3, May 2014.

[ZKZ13] Y.T. Zhu; T. Kang; T.K. Zhang; Z.M. Zeng, "QoS-aware user association based on cell zooming for energy efficiency in cellular networks", in proc.Personal, Indoor and Mobile Radio Communications (PIMRC Workshops),2013.